NASA/CR-2002-211671

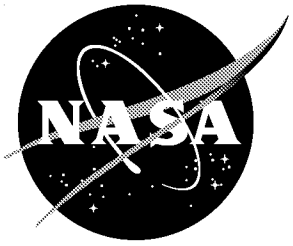

Analytical Simulations of Energy-Absorbing Impact Spheres for a Mars Sample Return Earth Entry Vehicle

Marcus Dwight Billings
Joint Institute for Advancement of Flight Sciences
The George Washington University
Langley Research Center, Hampton, Virginia

May 2002

The NASA STI Program Office ... in Profile

Since its founding, NASA has been dedicated to the advancement of aeronautics and space science. The NASA Scientific and Technical Information (STI) Program Office plays a key part in helping NASA maintain this important role.

The NASA STI Program Office is operated by Langley Research Center, the lead center for NASA's scientific and technical information. The NASA STI Program Office provides access to the NASA STI Database, the largest collection of aeronautical and space science STI in the world. The Program Office is also NASA's institutional mechanism for disseminating the results of its research and development activities. These results are published by NASA in the NASA STI Report Series, which includes the following report types:

- TECHNICAL PUBLICATION. Reports of completed research or a major significant phase of research that present the results of NASA programs and include extensive data or theoretical analysis. Includes compilations of significant scientific and technical data and information deemed to be of continuing reference value. NASA counterpart of peer-reviewed formal professional papers, but having less stringent limitations on manuscript length and extent of graphic presentations.

- TECHNICAL MEMORANDUM. Scientific and technical findings that are preliminary or of specialized interest, e.g., quick release reports, working papers, and bibliographies that contain minimal annotation. Does not contain extensive analysis.

- CONTRACTOR REPORT. Scientific and technical findings by NASA-sponsored contractors and grantees.

- CONFERENCE PUBLICATION. Collected papers from scientific and technical conferences, symposia, seminars, or other meetings sponsored or co-sponsored by NASA.

- SPECIAL PUBLICATION. Scientific, technical, or historical information from NASA programs, projects, and missions, often concerned with subjects having substantial public interest.

- TECHNICAL TRANSLATION. English-language translations of foreign scientific and technical material pertinent to NASA's mission.

Specialized services that complement the STI Program Office's diverse offerings include creating custom thesauri, building customized databases, organizing and publishing research results ... even providing videos.

For more information about the NASA STI Program Office, see the following:

- Access the NASA STI Program Home Page at ***http://www.sti.nasa.gov***

- E-mail your question via the Internet to help@sti.nasa.gov

- Fax your question to the NASA STI Help Desk at (301) 621-0134

- Phone the NASA STI Help Desk at (301) 621-0390

- Write to:
  NASA STI Help Desk
  NASA Center for AeroSpace Information
  7121 Standard Drive
  Hanover, MD 21076-1320

NASA/CR-2002-211671

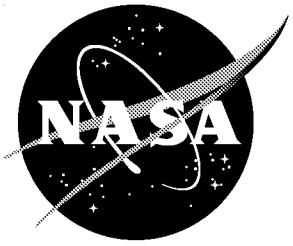

Analytical Simulations of Energy-Absorbing Impact Spheres for a Mars Sample Return Earth Entry Vehicle

Marcus Dwight Billings
Joint Institute for Advancement of Flight Sciences
The George Washington University
Langley Research Center, Hampton, Virginia

National Aeronautics and
Space Administration

Langley Research Center
Hampton, Virginia 23681-2199

Prepared for Langley Research Center
under Cooperative Agreement NCC1-01017

May 2002

Available from:

NASA Center for AeroSpace Information (CASI)
7121 Standard Drive
Hanover, MD 21076-1320
(301) 621-0390

National Technical Information Service (NTIS)
5285 Port Royal Road
Springfield, VA 22161-2171
(703) 605-6000

Abstract

Nonlinear dynamic finite element simulations have been performed to aid in the design of an energy-absorbing impact sphere for a highly reliable, passive Earth Entry Vehicle (EEV) that will be used in one possible architecture of the Mars Sample Return (MSR) mission. Materials from asteroids, comets, or planets can be returned to Earth for scientific analysis using an EEV. The MSR EEV concept uses an entry capsule and energy-absorbing impact sphere designed to contain and limit the acceleration of collected samples during Earth impact. The spherical shaped impact sphere is composed of solid hexagonal and pentagonal foam-filled cells with hybrid composite, graphite-epoxy/Kevlar cell walls. Collected Martian samples will fit inside a smaller spherical sample container at the center of the EEV's cellular structure. Comparisons were made of analytical results obtained using MSC.Dytran with test results obtained from four impact tests performed at NASA Langley Research Center for impact velocities ranging from 30 to 40 m/s. Acceleration, velocity, and deformation results compared well with the test results. The correlated finite element model was then used for simulations that investigated the cellular structure dynamic response to various off-nominal impact scenarios. Off-nominal simulations included impacting a rotated cellular structure into a flat surface, a cellular structure impact into an angled surface, and a cellular structure impact into the corner of a step, all at an impact velocity of 40 m/s. The analytical results provided increased insight into the dynamic behavior of the cellular structure and identified areas for further study.

Acknowledgements

I would like to express my sincere thanks to Dr. Edwin (Ed) Fasanella for his direct input towards my research. Over the last two years, Ed has been there on a day-to-day basis to offer suggestions, guidance, and insight into the direction of my research. Without his help, this research would never have progressed to completion. His guidance and suggestions in modeling the cellular structure, analyzing the data, and documenting the research have been invaluable.

I would also like to express my appreciation to Dr. Paul Cooper for his guidance and support over my tenure at GWU. Without his insight and thoughtful questioning, I would not have reached my current level of knowledge.

This research is a portion of the investigation being performed by the Mars Sample Return Earth Entry Vehicle Advanced Technology Development Group at NASA Langley Research Center. I would like to thank the entire team for their input over the duration of this research. Particularly, I would like to thank Dr. Robert A. Mitcheltree and Dr. Robert A. Dillman for their overall direction of the team.

The input and guidance of Dr. Sotiris Kellas has been invaluable to the progress of my research. I would like to thank Dr. Kellas for sharing his knowledge about the cellular structure concept in the areas of theory, design, fabrication, and testing, as well as providing material properties for the finite element models. I would also like to thank Yvonne Jones for her help in modeling components of the impact test specimens. Additionally, I would like to thank the entire group at the Impact Dynamics Research Facility for their support during this project.

Table of Contents

List of Figures

List of Tables

Nomenclature

cm ..... Center of Mass

CS ..... Cellular Structure

CV ..... Containment Vessel

E ..... Young's Modulus, Pa (N/m^2)

EEV ..... Earth Entry Vehicle

ε ..... Strain

ε_f ..... Plastic Strain Failure Limit

ε_p ..... Plastic Strain

IDRF ..... Impact Dynamics Research Facility

kg ..... Kilogram

m ..... Meter

mm ..... Millimeter

m/s ..... Meters per second

MSC ..... MSC.Software Corporation

MSR ..... Mars Sample Return

N ..... Newton ($kg*m/s^2$)

ν ..... Poisson's Ratio

OS ..... Orbiting Sample

ρ ..... Density, kg/m^3

s ..... Second

σ ..... Stress, Pa (N/m^2)

YS ..... Yield Stress, Pa (N/m^2)

UTTR ..... Utah Test and Training Range

1.0 Introduction

An Earth Entry Vehicle (EEV) is designed to return materials from asteroids, comets, or planets for scientific analysis on Earth [1-3]. In one possible architecture of the Mars Sample Return (MSR) mission, the collected Martian samples enter the Earth's biosphere and land on the surface using an EEV. One concept for an EEV is a circular aeroshell structure approximately one meter in diameter with an energy-absorbing impact sphere at the center of the vehicle. A simple, highly reliable, and cost-effective EEV would be a vehicle that has a direct entry to Earth and can withstand a terminal velocity land impact without external devices, such as a parachute, to reduce descent velocity. In addition, an optimal impact surface for an EEV would be soft soil [4]. Design criteria for the EEV concept require that sample containment be assured with a high level of reliability. Thus, an energy-absorbing impact sphere has been designed to limit the acceleration of the samples and provide the high level of reliability required for containment assurance.

The concept of the energy-absorbing impact sphere is a composite cellular structure made with energy-absorbing materials that limit the acceleration of the Martian samples. The cellular structure is composed of cells that are filled with energy-absorbing foam and enclosed with hybrid composite, graphite-epoxy/Kevlar cell walls. Energy-absorbing materials include carbon foam, Kevlar, graphite, and graphite-epoxy/Kevlar composites [5]. Rock, soil, and atmospheric samples are kept within the cellular structure in a sample container designated the orbiting sample (OS).

The required reliability and containment assurance criteria are being addressed, in part, by performing nonlinear dynamic finite element simulations of the impact of the EEV's cellular structure onto a rigid surface. These simulations serve as an aid in the design and testing phase

of the program. The purpose of the simulations was to calculate accelerations, velocities, and deformations of the cellular structure and compare with test results. Once confidence in the model was achieved, off-nominal impact scenarios were simulated that would otherwise prove to be difficult and costly to perform. These simulations were executed using the commercial nonlinear dynamic finite element code MSC.Dytran [6].

The objective of this thesis is to describe the modeling and simulation of the high-speed impact of the EEV cellular structure, to show comparisons of test data with numerical results, and to present off-nominal impact simulations and results. Each finite element impact model created for analysis will be described and compared with available test results from the corresponding drop test performed at the NASA Langley Research Center Impact Dynamics Research Facility (IDRF) [7]. In addition to modeling the specific cellular structure, a technique for modeling a very complex engineering system and simulating the high-speed impact is described.

2.0 Background

Detailed research has been performed in the areas of sample return missions, energy-absorbing concepts, and impact analysis of complex systems. To understand the current level of knowledge for these concepts, a literature search was performed and summarized.

2.1 Sample Return Missions

Returning samples from asteroids, comets, or planets to the Earth's surface for analysis will greatly enhance our knowledge of the universe and possibly give clues to how life began on Earth [8]. This engineering challenge has been studied and analyzed for space missions designed

to accomplish various objectives. In upcoming years, samples of comet particles (Stardust), solar wind particles (Genesis), and asteroids (Muses-C) will be returned to the surface of Earth for scientific analysis. In addition, it is widely believed that before sending humans to Mars, greater knowledge of the Martian atmosphere and soil, as well as the possible presence of water, is needed. This knowledge can be increased with a Mars Sample Return mission that will return selected Martian samples to Earth in the most reliable and safe manner. With Martian samples here on Earth, detailed microanalyses can be performed to vastly increase the scientific knowledge of Mars.

The final portion of the Mars Sample Return mission is the entry of the EEV into the Earth's biosphere for recovery. This has been a topic of numerous studies [1-3]. The primary requirement is to assure containment of the returned samples within the EEV. This containment would isolate the Mars samples from Earth based contamination and protect the Earth's biosphere from possible, however unlikely, pathogens from Mars. Although extremely small, the National Research Council's Task Group on Issues in Sample Return has determined that the potential for terrestrial contamination from Martian samples is not zero [9]. Thus, a reliable, passive, Earth Entry Vehicle, with minimal failure modes and sufficient redundancy and robustness, must be designed to adequately return samples to the Earth's surface [3]. A concept for the MSR EEV for a direct Earth entry is shown in Figure 1.

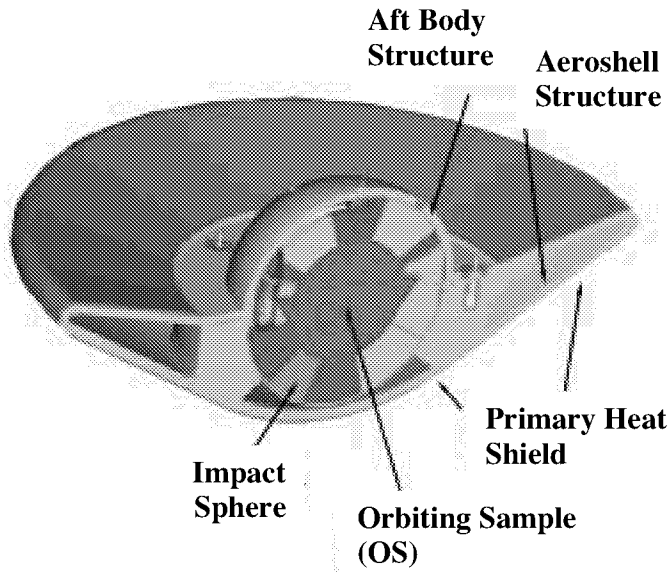

Figure 1 – Schematic of candidate Earth Entry Vehicle (EEV).

2.2 Energy Absorption Methods

To help satisfy the containment assurance criterion, an energy-absorbing impact sphere has been designed to contain and cushion the returning Martian samples for a direct entry impact. The nominal landing site for the EEV is the Utah Test and Training Range (UTTR), which is a large, government controlled area containing a dry lakebed consisting of moist, soft soil. If all mission objectives are met, the combination of the soft soil and the EEV energy-absorbing materials will dissipate the impact energy, assuring containment of the Mars samples. Dynamic ground characterization tests of UTTR soil have been performed for the Mars Sample Return mission [1-3,8] as well as dynamic finite element studies of penetrometer impact into the soft soil [4]. Agreement between test and analysis has provided a design tool that will predict peak acceleration on the vehicle given the mass, diameter, and impact speed of the EEV.

Surrounding the UTTR landing site are mountains, roads, rocks, and concrete pads, to name a few obstructions. The probability of an EEV impact into these obstacles can not be considered zero. To contain the samples in the unlikely event the EEV impacts these obstacles [3], an energy-absorbing impact sphere has been designed [5] using rigid foams, graphite-epoxy/Kevlar hybrid composites, and Kevlar fabric. The design was based on a cellular concept in which blocks of foam were wrapped in a graphite-epoxy/Kevlar composite and then assembled to form a structure. The impact sphere design has been adapted from previous studies in which a similar concept was used to absorb the crash impact energy of light airplanes to improve crashworthiness [10-13].

The designed energy-absorbing impact sphere was fabricated and tested five times at the Impact Dynamics Research Facility (IDRF) at NASA Langley Research Center. Each controlled test provided knowledge on how the impact sphere would dynamically respond to a hard surface impact. The impact test was performed to verify the concept and show that the concept could satisfy the maximum acceleration criterion for a hard surface impact. Additionally, each impact test provided data that allowed for correlation of the dynamic finite element model described in this paper. Details of each test can be found in reference [5].

2.3 Impact Finite Element Analysis

To further satisfy the containment assurance criteria set forth by mission requirements, finite element analyses were performed of the energy-absorbing sphere impacting a rigid surface. Previous studies in the area of impact modeling of complex systems and materials, such as foams and composites, have focused on aircraft and helicopter sections. These studies were performed to build confidence in the impact finite element codes as a tool for crashworthy design and

evaluation [14-16]. Detailed analyses have also been performed on specific composite structures such as subfloor beams, constructed of foam and composite panels, for crashworthy design applications [17,18]. In these studies, the identified areas of improvement were in the development of accurate material models for material failure and degradation as well as improved contact formulations. In spite of the current challenges, correlation between experimental data and analytical results for this study has generally been good.

3.0 Research Description

The first goal of this research was to generate a finite element model of the Mars Sample Return cellular structure impact test specimen that could be used in simulations of the impact tests conducted at the IDRF. The ability to perform finite element analysis of the energy-absorbing impact sphere into a hard surface and to validate the model with experimental data would be useful to the EEV design team. Currently, five impact tests have been performed. Four tests, designated #1, #2, #3, and #4b in reference [5], have provided acceptable data for correlation purposes. For simplification, test #4b in reference [5] will be designated as test #4 in this report. The four impact tests and the corresponding impact models will be described in this report.

The second goal of this research was to perform off-nominal impact simulations to determine how the cellular structure might dynamically respond to an impact on various hard surfaces. With the dynamic finite element model correlated using four impact tests, the model can be used to study impacts in the same velocity regime at different impact attitudes and on different geometric surfaces. Numerous impact cases can be simulated that would take a fraction of the time and cost associated with an impact test. With these off-nominal impact studies,

insight into the performance of the cellular structure onto surfaces other than flat and horizontal can be investigated. Included in this report is an off-nominal impact study showing the dynamic response of the cellular structure to three different surfaces.

4.0 Impact Finite Element Analysis Code

All finite element analyses were performed using the finite element code MSC.Dytran. MSC.Dytran is an explicit nonlinear transient dynamic finite element computer code used for analyzing solid components, structures, and fluids [6]. The primary use for MSC.Dytran is the computation of short duration, highly nonlinear, impact and crash simulations in the areas of automobile crash and aircraft crashworthiness analysis. The origins of MSC.Dytran can be traced to the public domain code DYNA3D developed at the Lawrence Livermore National Laboratory. MSC first marketed an explicit finite element code called MSC/DYNA based on the 1988 version of DYNA3D. In 1991, MSC combined the Lagrangian solver available with MSC/DYNA and the Eulerian solver available in MSC/PISCES to provide the analysis tool, MSC/Dytran. Over time, the code has been updated and modified many times, to the current version of the code, MSC.Dytran 2000 [6,19].

MSC.Dytran is an explicit code that uses central difference integration to solve the problem in time and Lagrange-finite element technology to solve the problem in space. At each time-step, or cycle, the explicit solver applies the solution method to each individual element in the model. In contrast, a finite element code that uses an implicit solver determines a global solution by formulating a global stiffness matrix, reducing and inverting the matrix, and solving for grid-point positions. The explicit method begins by evaluating any applied boundary conditions to the elements. An element strain increment is determined from the boundary

conditions using the element formulation. An element constitutive model is then used to calculate the stress on the element and sums the stresses to determine the new total stress. The internal element forces are then updated using the updated element stress. The total force (internal plus external) is then applied to each grid-point. Each grid-point acceleration is calculated by dividing the grid-point force by the grid point mass, eliminating the need for matrix inversion. Using the central difference integration, grid-point velocity and position is calculated and updated. The time is updated and a check is performed to determine if the simulation is terminated. The cycle then repeats and the process moves forward in time until the maximum time limit has been reached.

The time-step for the explicit finite element simulation is automatically calculated and is set by the requirement to ensure stability of the central difference method. In essence, the time-step must be smaller than the time it would take a stress wave to propagate through the smallest element. In MSC.Dytran, the equation used to calculate the time step is based on the smallest element dimension divided by the speed of sound for that element. The speed of sound is defined by the square root of the quantity of Young's Modulus divided by density.

The code offers a library of relatively simple structural elements including beams, bars, rods, shells, and solids for modeling complex structures. The one-dimensional elements are defined using two grid-points and offer two element formulations, Belytschko-Schwer and Hughes-Liu. The shell elements are defined with four grid-points and offer various element formulations, such as Belytschko-Tsay, Hughes-Liu, and Key-Hoff. The solid hexagonal elements contain eight grid-points with a single point Gauss integration at the element center to determine the stresses. Additionally, springs, dampers, and lumped masses can be defined to complete the finite element model. For efficiency, elements that contain mid-side grid-points or

more than one integration point through the thickness are not available in the explicit finite element code.

MSC.Dytran also offers a variety of material models for elastic and elastic-plastic materials where element failure and elastic hardening can be defined. A typical stress-strain curve for this material model is shown in Figure 2. Additionally, there are a number of crushable foams and soil models that allow for the definition of materials that have an effective Poisson's ratio of zero or exhibit nonlinear crushable material properties. Included with the material definition are the types of available yield models. In MSC.Dytran, a Hydrodynamic Yield Model, Von-Mises Yield Model, Johnson-Cook Yield Model, and Mohr-Coulomb Yield Model are available. Additionally, within each material model, element failure can be defined in a number of ways depending on the element formulation or the type of failure desired. Available failure models are Tsai-Hill, Tsai-Wu, Modified Tsai-Wu, Maximum Stress, Maximum Plastic Strain, Chang-Chang, or even a used defined failure model.

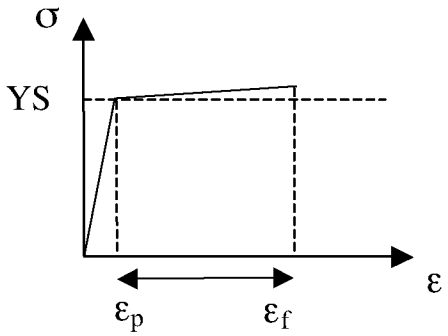

Figure 2 – Stress-strain curve for a bilinear elastic-plastic material model with defined failure.

Most simulations that use the explicit finite element method have a contact surface defined in which a portion of the model will interact with the defined contact surface. Several options are available within the contact algorithm for the master-slave interaction, such as master

surface-slave surface contact, single surface contact, and master surface-slave node contact. The contact formulation uses the penalty method to determine contact forces at the master-slave interface. The algorithm evaluates if a slave node has penetrated a master surface. Based on slave node penetration depth, an effective mass, the element normal length, and the current time-step, a contact force is calculated to move the node back to the master surface. Also included is the ability to define a contact force scale factor and static and dynamic friction values between master and slave surfaces

Archive files for post-processing deformed shapes and time history files for viewing element results must be requested by the user in advance. Available outputs for model post-processing include grid-point accelerations, velocities, and positions; element stresses and forces; and element contact forces. A restart capability is also provided.

5.0 Cellular Structure Concept

Impact tests of the cellular structure specimens were conducted at the IDRF to evaluate and optimize energy absorption and to ensure sample containment within the OS [1]. To preserve the scientific integrity of the collected samples, a design criterion requires that the OS peak acceleration upon impact be limited to 2,500 g's. In addition, the OS peak acceleration must not exceed 3,500 g's on a hard surface impact to ensure sample containment [3]. Additionally, the cellular structure must not completely crush on impact. For each test, variations were made to cell wall thickness, foam density, and/or OS size and shape. A cross-section representing a typical impact test specimen used in the three drop-tests is shown in Figure 3. A cross-section representing the impact test specimen used for the fourth drop test is shown in Figure 4.

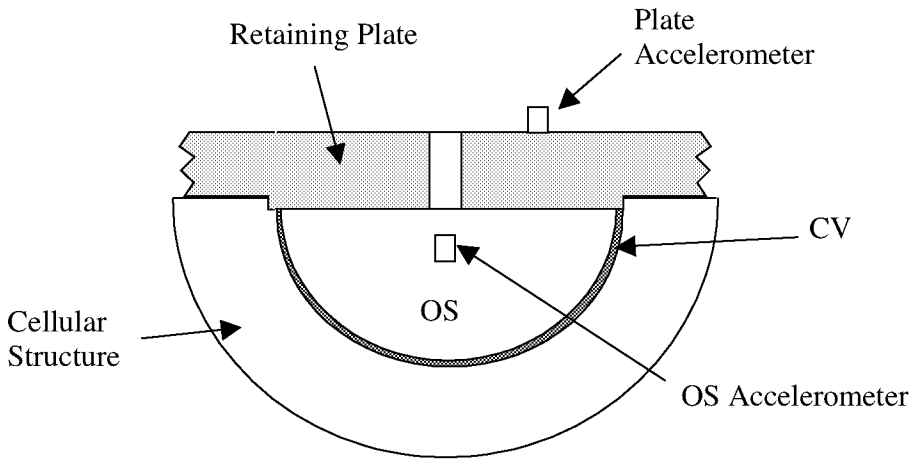

Figure 3 – Typical impact test specimen for tests #1, #2, and #3.

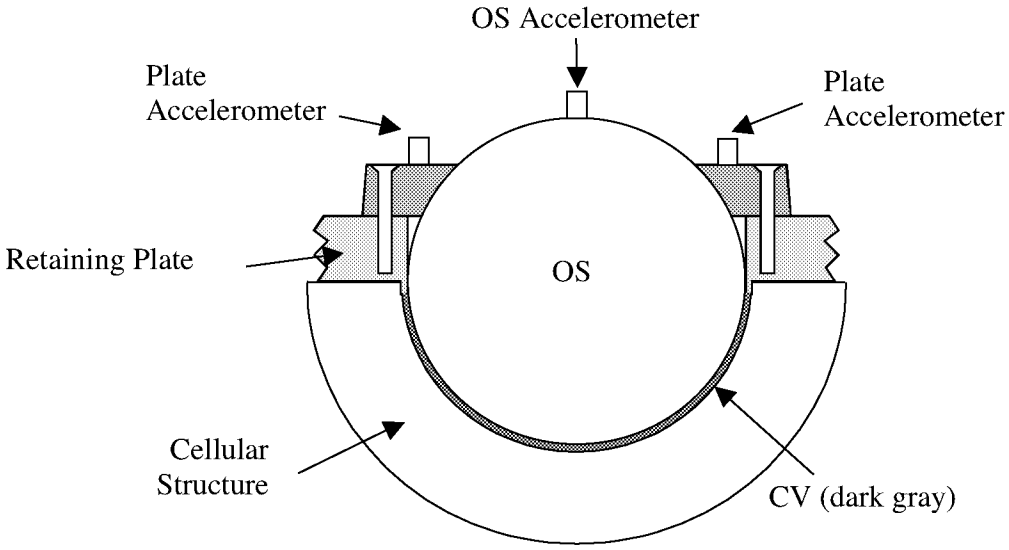

Figure 4 – Typical impact test specimen for test #4.

The impact test specimen was a hemispherical-shaped structure with six pentagonal shaped cells, five hexagonal shaped cells, and ten hexagonal shaped cells on the equator that were cut to form the hemisphere. The bottom view of a typical cellular structure is shown in Figure 5, which illustrates how the individual cells were assembled to form the complete cellular structure.

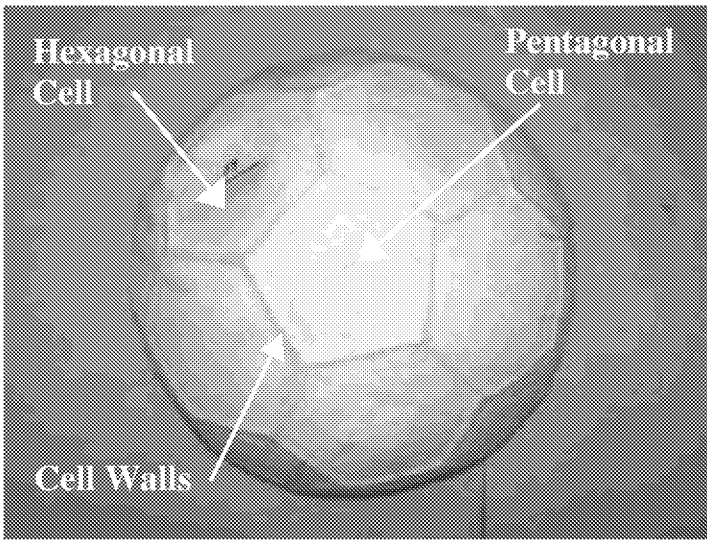

Figure 5 – Bottom view of cellular structure showing shape and geometry of cells.

Each foam-filled cell had hybrid composite, graphite-epoxy/Kevlar cell walls. The graphite-epoxy laminates provided stiffness and strength, while the Kevlar layers provided structural integrity. Polyurethane foam was used initially to demonstrate the concept. It was later replaced with carbon foam, which will be used in the flight vehicle, but was used sparingly due to high cost. The outer surface of the cellular structure was wrapped in Kevlar, while the inner surface, which supports the OS, was constructed of a graphite-epoxy laminate. Between the larger cellular structure and the OS were several layers of woven Kevlar fabric, which form the Containment Vessel (CV). The Kevlar was layered inside the cellular structure to provide additional containment and to increase penetration resistance from foreign objects. The OS will contain materials collected from the Mars exploration mission, i.e., rock, soil, and atmospheric samples. Two options are being considered for the OS design. One has strong structural foam surrounding a titanium canister, which contains and protects the samples over the course of the mission. The other concept has the OS constructed of a metallic alloy that is yet to be

determined. A retaining plate was also added to the impact test specimen and represented the mass associated with the top half of the cellular structure, which was not constructed for the impact test program. The components of a typical drop test specimen can be viewed in Figure 6. A picture of an assembled impact test specimen is shown in Figure 7.

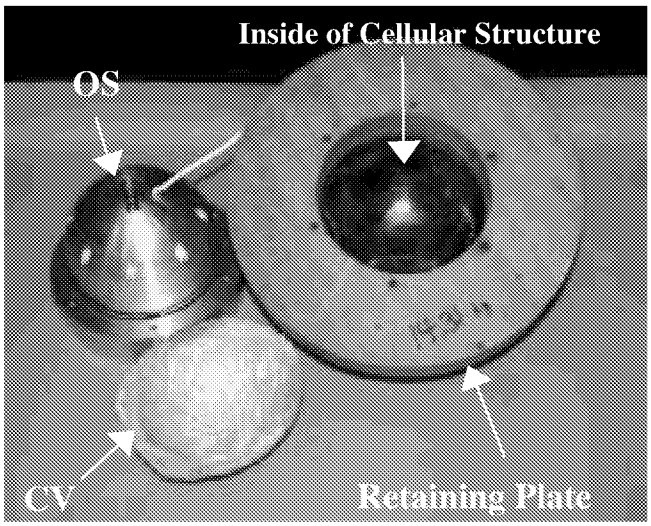

Figure 6 – Picture showing components of impact test specimen.

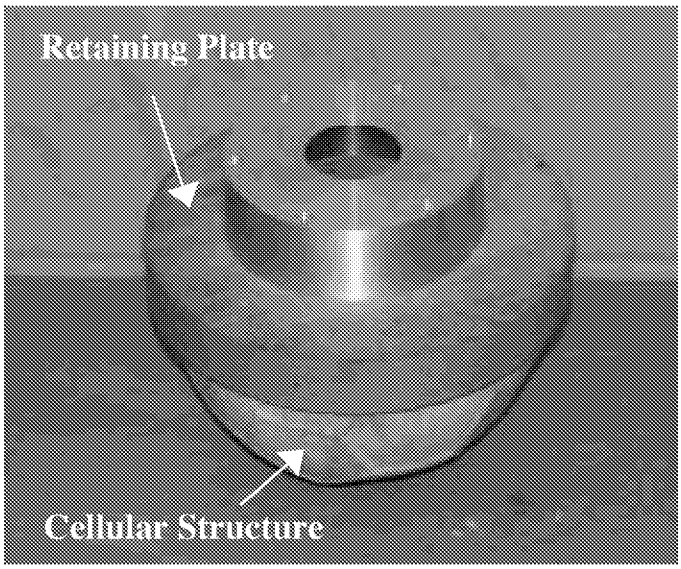

Figure 7 – Picture of typical impact test specimen with OS located within cellular structure.

6.0 Impact Dynamics Research Facility

The first two cellular structure impact tests were instrumented drop-tests from the 73 meter high gantry structure at the IDRF [7]. Impact test specimens were dropped from the gantry, which generated impact velocities up to 32 m/s. A picture of the IDRF is shown in Figure 8. A bungee assisted accelerator system was then designed and constructed at the IDRF gantry to produce impact speeds up to approximately 40 m/s, the expected terminal velocity of this EEV concept. A diagram of the bungee accelerator is illustrated in Figure 9. To meet the goals of this research, the modeling of four separate impact tests is described illustrating development of the cellular structure concept. Table 1 outlines the four impact tests with pertinent test parameters provided. For complete details of each impact test, see reference [5]. For simplification, test #4b in reference [5] will be designated as test #4 in this report.

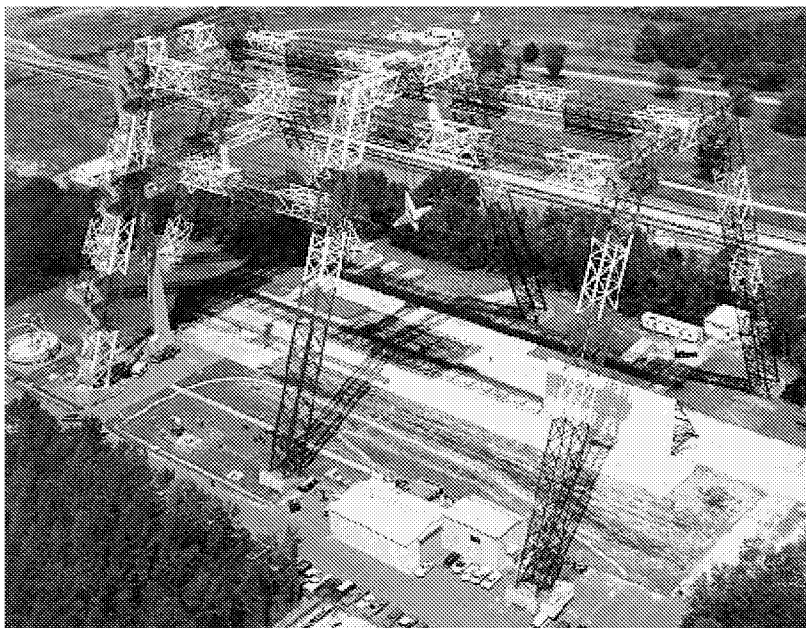

Figure 8 – Impact Dynamics Research Facility at NASA Langley Research Center.

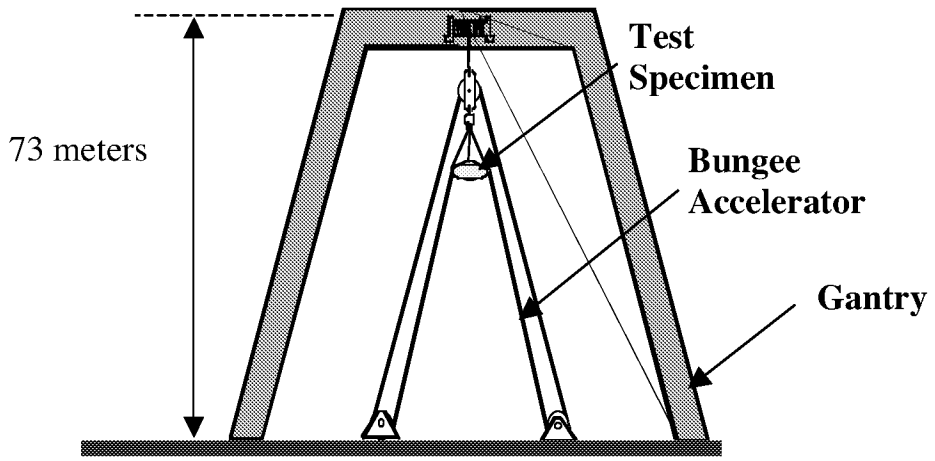

Figure 9 – Schematic drawing of bungee accelerator located under gantry structure.

Table 1 – Impact parameters of drop test specimens

Drop Model	Total Mass (kg)	Impact Velocity (m/s)
1	9.85	32.0
2	9.30	30.3
3	12.38	35.5
4	14.31	40.4

7.0 Impact Simulation #1

This initial impact test was used to establish a method for dynamic testing of the cellular structure concept. The test results were also used to validate the design of the concept and provided information for the design of future cellular structure impact test specimens. The specimen was dropped from the gantry and had an impact speed of 32 m/s. The cellular structure/retaining plate had a mass of 6.16 kg and the OS had a mass of 3.69 kg, resulting in a total mass for the first drop test of 9.85 kg. Including the Kevlar outer shell, the cellular structure had an outside diameter of 0.314 m and including the graphite-epoxy inner shell, had an inside diameter of 0.178 m. The CV thickness was approximately 5.6 mm. One accelerometer was mounted inside the impact test specimen to determine the OS response, and the second was

mounted on top of the back retaining plate, as shown in Figure 3. Additionally, a low-g accelerometer was used to determine the impact speed. High-speed film and digital video were also used to capture the impact event.

7.1 Finite Element Model #1

The major components of the impact test specimen were the cellular structure, the CV, and the OS. The components of the cellular structure were the energy-absorbing foam, the composite cell walls, the inner graphite-epoxy shell, and the outer Kevlar shell. The CV and OS were defined separately. The sample containing OS that is within the cellular structure was represented by rigid body shell elements located on top of the CV. Concentrated masses were applied at various locations across the top of the cellular structure to model the back retaining plate, which represents the top half of the energy-absorbing cellular structure. The impact surface was modeled with shell elements. Failure was not defined for any elements in the first model. This constitutes the baseline finite element model for the impact analysis. The discretized model that was used to simulate the first impact test is shown in Figure 10. An exploded view of the impact model showing the major components is shown in Figure 11.

The MSC.Dytran model contained 4,635 grid-points and 6,610 elements. The model consisted of seven groups of elements, including the foam in each cell, the graphite-epoxy/Kevlar cell walls, the inner and outer shell of the cellular structure, the CV, the rigid body OS, and the impact surface.

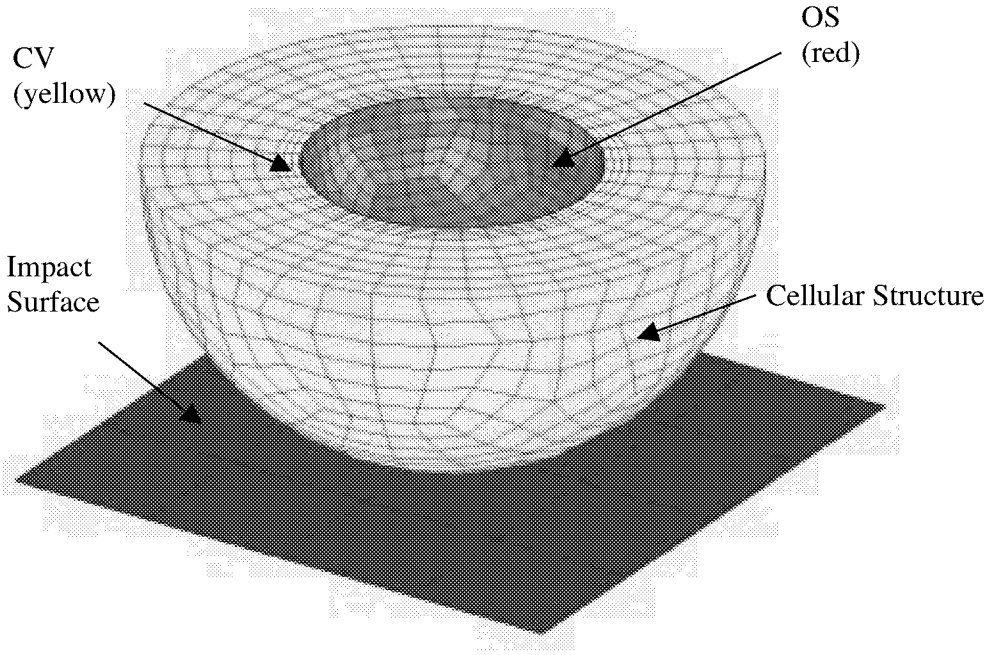

Figure 10 – Components of finite element model #1.

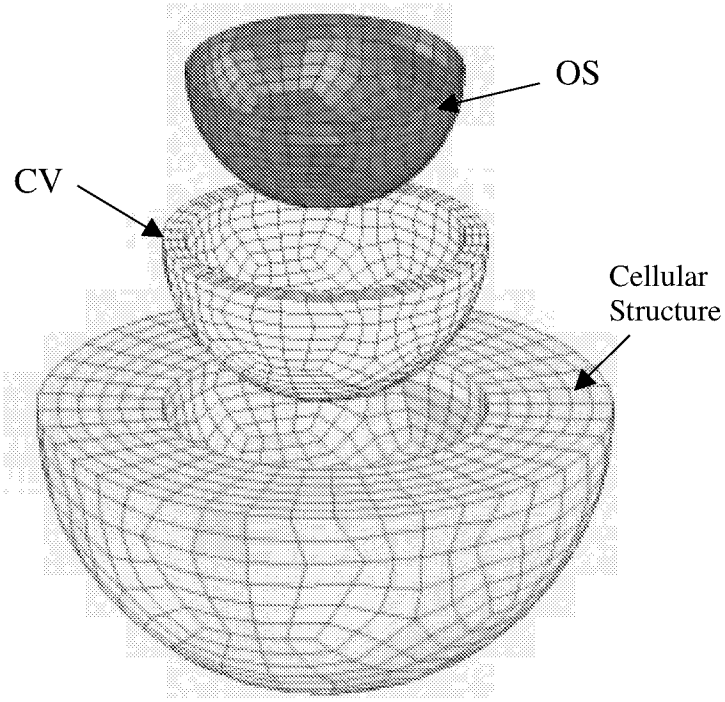

Figure 11 – Exploded view of finite element model #1.

The polyurethane foam cores were modeled using 8-node Lagrangian solid elements. The material model for these elements was an isotropic, elastic-plastic material model with a bilinear stress-strain curve, no defined hardening modulus, and a yield stress defined to allow for plastic deformation. In this analysis, isotropic material properties for the foam were based on testing of foam core samples [5].

To define the graphite-epoxy/Kevlar cell walls, 4-node Lagrangian shell elements were used with an isotropic, elastic-plastic material model and a defined shell thickness. For the analysis, equivalent isotropic material properties for the cell walls were determined from multiple test coupons cut at different orientations from a large quasi-isotropic panel [5]. The coupons were statically tested and the results averaged to determine effective values. Figure 12 shows the shell elements used to discretize the cell walls.

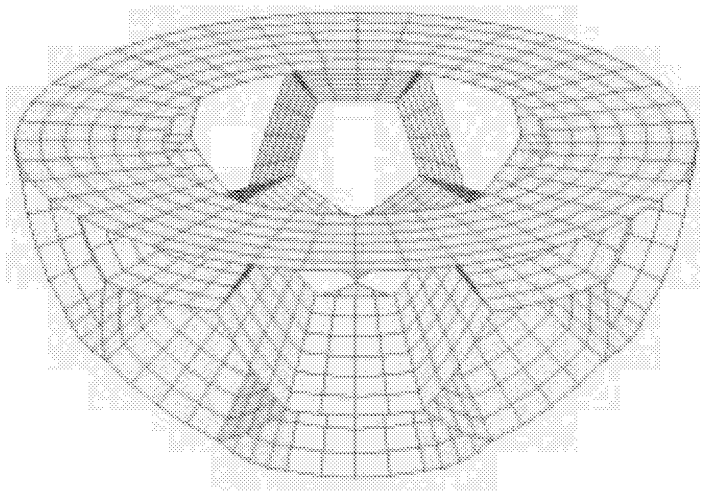

Figure 12 – Shell finite elements that define the cell walls.

The inner surface of the cellular structure was a laminate composite of graphite-epoxy material and was represented by 4-node shell elements and an equivalent isotropic, elastic-plastic

material model. For this set of elements, the thickness of the shells was defined to match the physical dimensions of the impact test specimen.

The outer hemispherical surface of the cellular structure was wrapped with Kevlar sheets and was modeled as an isotropic, elastic-plastic material and 4-node shell elements. For this set of elements, the thickness of the shells was defined to match the physical dimensions of the impact test specimen.

The CV was represented by 8-node Lagrangian solid elements. For each solid element, there is one integration point located at the center of the element. For improved prediction of the stress distribution through the CV, three elements were defined through the thickness. The material model for these elements was an isotropic, elastic-plastic model where the material values were based on the properties of woven Kevlar fabric. For the finite element model, the CV density was determined by dividing the mass of the CV by the volume calculated by the finite element code.

The OS was modeled using 4-node Lagrangian shell elements located on the top surface of the CV. These elements were defined as a rigid body and represented the mass and inertia associated with the OS. In the first impact test specimen, the OS was represented by ballast weight that filled the inner volume of the cellular structure. To represent the surrogate OS in the model, the rigid body shell elements were defined to have mass, a center of mass (cm), moments of inertia, and an initial velocity matching the test article.

Included in the model were concentrated masses distributed around the top of the cellular structure. These masses represented the weight associated with the retaining plate, which represented the top half of the cellular structure. For impact simulation #1, each lumped mass was defined to be 0.439 kg, resulting in 4.39 kg of total mass added to the model.

The impact surface was modeled using 4-node Lagrangian shell elements with a thickness of approximately one meter. The material model for these elements was an isotropic model used to represent the impact surface at the IDRF. The impact surface was modeled as deformable to avoid numerical difficulties in the contact algorithm when a surface is defined explicitly as a rigid surface.

The contact defined between the cellular structure and the impact surface was modeled using the penalty method with master surfaces and slave nodes. In the analysis, shell elements representing the impact surface were the master surfaces, and all nodes of the cellular structure were defined as slave nodes. At the beginning of the analysis, the cellular structure was positioned approximately one millimeter above the impact surface. This method ensured no initial penetration of slave nodes into the master surface upon starting the simulation.

Figure 13 shows a cross-section of the discretized impact test specimen used in the first impact simulation. A summary of the material properties used in the finite element model for impact simulation #1 can be found in Table 2.

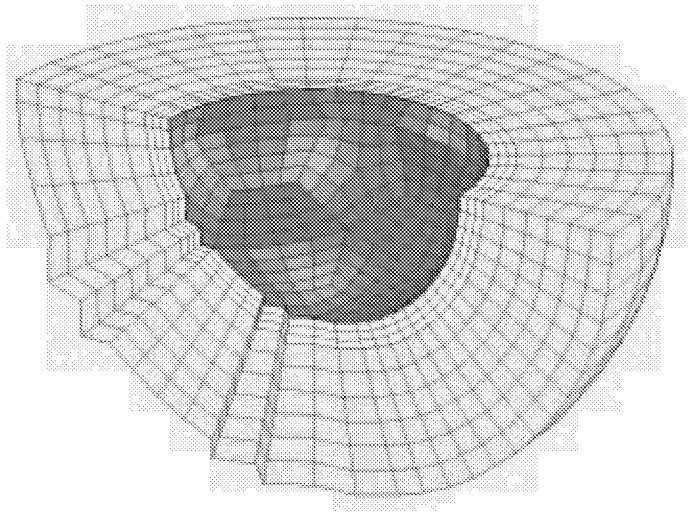

Figure 13 – Cross-section of finite element model #1.

Table 2 – Material property values used in finite element #1.

Material	Property Model	Material Model	Number of Elements	Density (kg/m^3)	Volume (m^3)	Mass (kg)
Cell Foam	PSOLID	DMATEP	2,640	85	6.60×10^{-3}	0.56
Cell Walls	PSHELL	DMATEP	1,320	1,539	6.28×10^{-4}	0.96
Inner Shell	PSHELL	DMATEP	440	1,550	3.77×10^{-5}	0.05
Outer Shell	PSHELL	DMATEP	440	1,379	7.74×10^{-5}	0.10
CV	PSOLID	DYMAT24	1,320	383	5.15×10^{-4}	0.19
OS	PSHELL	MATRIG	440	N/A	N/A	3.69
Concentrated Masses			10	N/A	N/A	4.39
Total Number of Elements			**6,610**	**Total Impact Mass**		**9.94**

Table 2 (continued)

Material	Young's Modulus ($\times 10^9$ Pa)	Poisson's Ratio	Yield Strength ($\times 10^6$ Pa)	Shell Thickness ($\times 10^{-3}$ m)
Cell Foam	0.02	0.3	1.034	N/A
Cell Walls	13.79	0.3	137.9	3.05
Inner Shell	45.50	0.3	579	0.76
Outer Shell	6.895	0.3	103.4	0.50
CV	70.00	0.3	34.4	N/A
OS	N/A	N/A	N/A	1.58

7.2 Numerical Results for Impact Simulation #1

The finite element simulation was executed using MSC.Dytran on a contemporary engineering workstation. The maximum time-step for impact simulation #1 was 0.1593 microseconds. The simulated impact was run for 0.004 seconds to capture the complete acceleration pulse. This resulted in 25,125 cycles or the number of times the model was updated during the simulation. After 0.004 seconds, the cellular structure has rebounded and the simulation was terminated. The finite element simulation took approximately three CPU hours with one cycle taking approximately 0.4 seconds to compute.

The intent of passing the acceleration curve through a low-pass filter is to extract the fundamental acceleration pulse from the analytical data. Generally, the analytical acceleration contained high-amplitude high-frequency components that were not present in the experimental data. A low-pass, 2nd order Butterworth filter was used to remove the high frequency ringing and extract the fundamental acceleration pulse from the analytical data. Forward and backward filtering was used to produce zero-phase distortion in time. To illustrate the point, Figure 14 shows the acceleration data for impact simulation #1 along with the filtered acceleration curve that was passed through a 2,500 Hz low-pass filter.

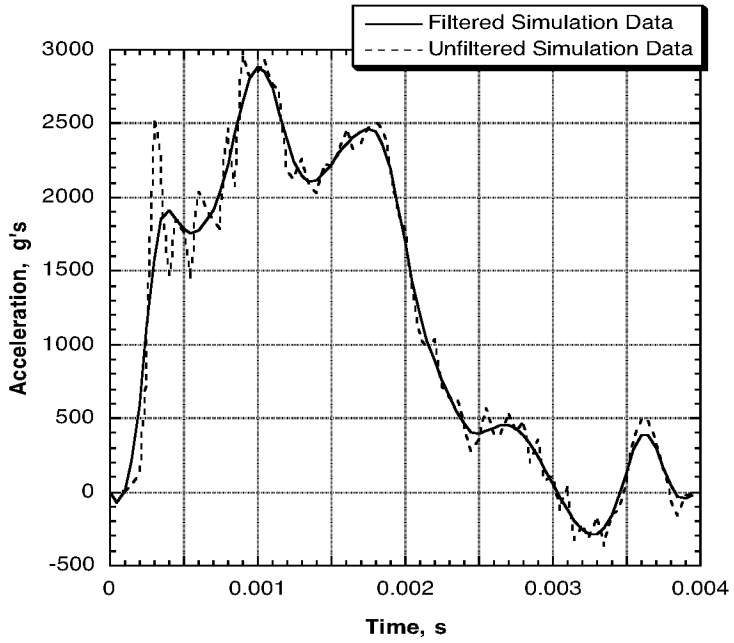

Figure 14 – Filtered and unfiltered acceleration data for impact simulation #1.

Data from the OS accelerometer was compared with the analytical acceleration response of the rigid body OS in Figure 15. Both the analytic and test OS accelerometer data were passed

through a 2,500 Hz low-pass filter to extract the fundamental acceleration pulse. The experimental peak acceleration of the OS was 2,500 g's and occurred at approximately 0.0007 seconds. The numerical simulation of the impact determined the peak acceleration on the OS to be approximately 2,900 g's, which occurred 0.001 seconds into the impact. After this time, the experimental acceleration decreases with the analytical acceleration data delayed by 0.0005 seconds. Although the analytical peak value was slightly higher, the overall shape and duration of the acceleration pulse compared favorably to the experimental acceleration pulse.

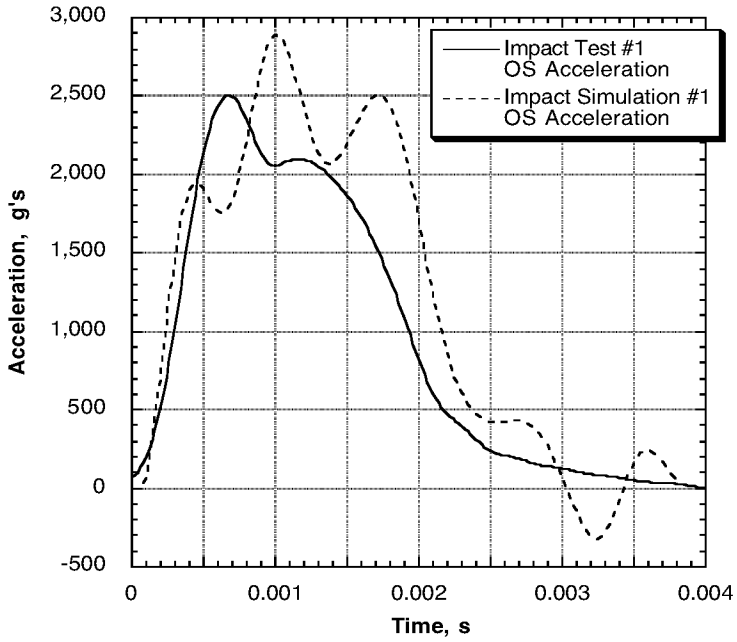

Figure 15 – Comparison of analytic and impact test acceleration for test #1.

Comparison of the analytic and experimental velocity of the cellular structure is shown in Figure 16. Velocity data from the impact test was calculated by integrating the experimental acceleration once. This data was compared with the analytic velocity output from Dytran. The

analytic data matched the test data well through the first half of the simulation. After this point, the numerical data shows a higher rebound velocity, eleven meters per second, than what was observed in the test, four meters per second. This higher predicted rebound velocity is representative of high amounts of elastic energy in the cellular structure and shows the need for additional energy absorption mechanisms in the finite element model.

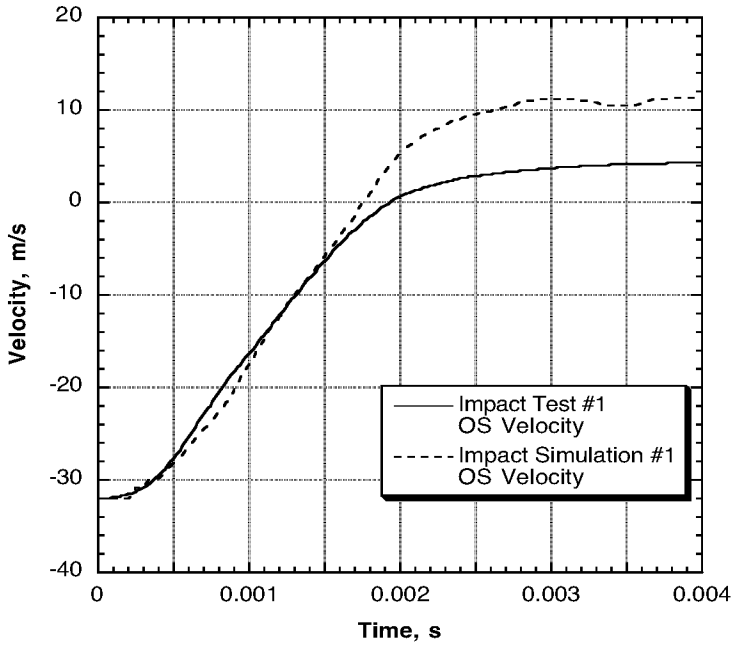

Figure 16 – Comparison of analytic and impact test velocity for test #1.

The crush stroke of the cellular structure was determined by the vertical displacement of the rigid body shells on top of the CV, which represent the OS. This displacement included the deformation of the CV, however the CV deformation was negligible (less than 5% of the total stroke) and was neglected. By monitoring the OS rigid body displacement, an efficient and consistent method of determining the cellular structure crush stroke is provided. Figure 17

shows the variation in displacement of the OS rigid body as determined by the simulation, and is compared with the impact test displacement determined by twice integrating the experimental acceleration data.

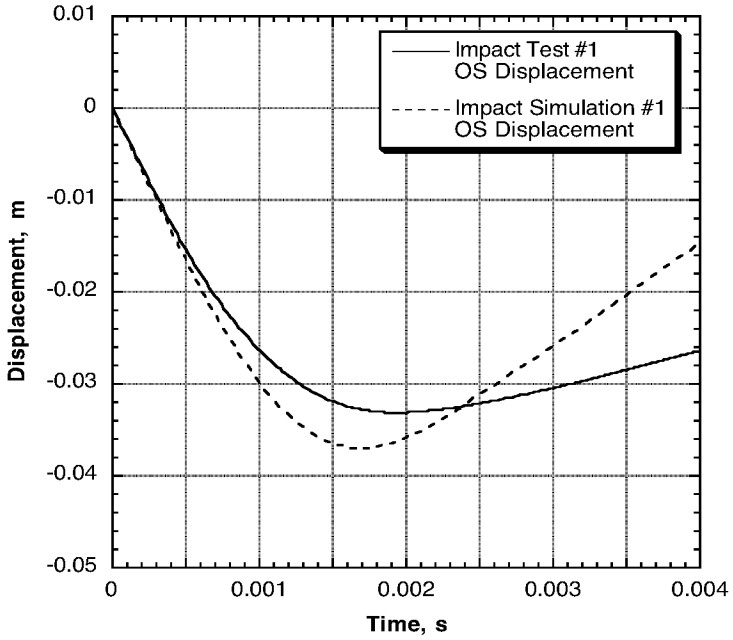

Figure 17 – Comparison of analytic and impact test displacement for test #1.

The finite element simulation of the impact predicted a total crush stroke of 37 mm, or 54% of the available 68 mm analytic crush distance. Data from the impact test showed that the cellular structure experienced a total crush stroke of 33 mm, or 49% of the available crush distance. Although these results indicated that the numerical model predicted conservative values, the analytic displacement data showed a larger amount of rebound during the 0.004 second impact. Again, this is representative of high amounts of elastic energy and the need for energy dissipation from the cellular structure model during the simulated impact. However, the

predicted maximum crush stroke only differed from the test by 6%, providing good correlation. A deformed plot of the cellular structure at maximum deformation is shown in Figure 18.

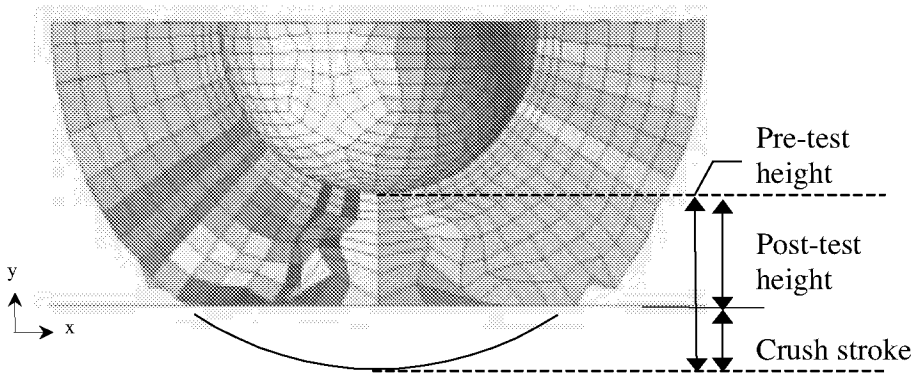

Figure 18 – Cross-section of deformed cellular structure #1, t = 0.002 s.

Data from the analytical acceleration, velocity, and displacement imply that an increased amount of elastic energy needs to be removed from the cellular structure model. One option of accomplishing this goal is to model the foam core material with a material model more indicative of observed foam material behavior. With the complexity of determining material failure strain values, element failure was also not defined for any elements in the model. Although these concepts were not used here, these options were explored in subsequent impact simulations as a method to remove energy from the cellular structure and more accurately predict the dynamic response.

8.0 Impact Simulation #2

The objective of the second, and final, free-fall drop test performed at the Impact Dynamics Research Facility was to determine the dynamic response of a cellular structure with

weaker cell walls used to support the same polyurethane foam core material used in the first drop test. Physical changes to the impact test specimen included a reduced number of plies for the composite cell walls, resulting in a reduced thickness of the cell walls from 3.05 mm to 2.03 mm. The cellular structure/retaining plate had a mass of 5.65 kg and the orbiting sample (OS) had a mass of 3.65 kg, resulting in a total impact test mass of 9.3 kg. The outside diameter of the cellular structure, including the layers of the Kevlar outer shell, was 0.315 m and the inside diameter, including the graphite-epoxy inner shell, was 0.176 m. The impact velocity of this test was determined by video analysis and found to be 30.3 m/s. For this experiment, two accelerometers were used to capture the dynamic loads transferred to the impact test specimen. One accelerometer was used to measure the surrogate OS response while the other accelerometer captured the acceleration of the retaining plate, as shown in Figure 3. Test data also determined that a small gap existed between the cellular structure and the OS upon impact. The cable used to transmit data from the OS accelerometer was severed at approximately 0.003 seconds into the impact, thus limiting the amount of available test data. However, enough information was captured to make meaningful comparisons between analytical and test data.

8.1 Finite Element Model #2

With minimal changes made to the cellular structure, there were few changes required of the baseline finite element model. Modeling of the second cellular structure was unchanged from the first model with the following exceptions that were made to the second test specimen. In the model, the thickness of the cell walls was reduced to 2.03 mm as a result of the change in the number of plies in the composite cell walls. The design change also modified the effective yield stress of the cell walls, which was reduced to 1.145×10^8 Pa.

Modeling of the polyurethane foam cores was updated by replacing the elastic-plastic material model with a foam material model where the Poisson's ratio is effectively zero. The FOAM1 material model was developed to more accurately represent foam crushing. The elastic-plastic material model used in model #1 allowed for lateral, elastic deformation of the foam material. Because of this lateral, elastic deformation, excessive elastic energy might have been stored in the elements, resulting in the high rebound velocity observed in the first impact simulation. A user-defined stress-strain curve was implemented in conjunction with the FOAM1 material model to represent the piecewise linear stress-strain curve of the polyurethane foam. Figure 19 shows a representative stress-strain curve used to define the foam material behavior with elastic, sustained crush, and compaction zones defined.

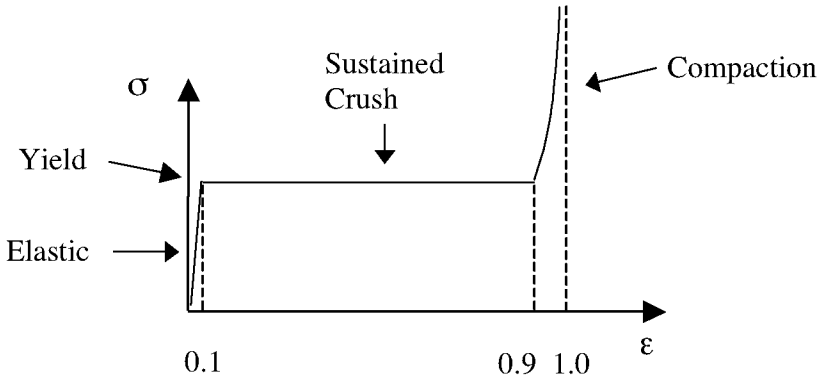

Figure 19 – Typical stress-strain curve defined for the FOAM1 material model.

The foam material data was acquired from a quasi-static crush test of the foam cores [5] and was defined to have an increase in stress due to compaction of the foam material after approximately 90% strain. This large compaction stress is also required to prevent the solid elements from turning "inside out", which `produces negative volumes and a fatal error during the simulation. Since the Poisson's ratio is effectively zero, only one other elastic constant was

needed. For the polyurethane foam material, a bulk modulus of 6.61 x10^6 Pa was used. The polyurethane foam had a density of 85.78 kg/m^3 and a yield stress of 1.034 x10^6 Pa.

The overall mass for the second impact test specimen was decreased from 9.82 to 9.30 kg. In the previous model, localized deformation associated with each lumped mass was observed on the top surface of the cellular structure. To remove the localized deformation, the concentrated masses were distributed over 30 nodes around the top of the model. Each lumped mass was 0.135 kg, resulting in 4.05 kg of total mass added to the model.

8.2 Numerical Results for Impact Simulation #2

The simulation was executed for 0.004 seconds for an expected impact pulse of approximately 0.003 seconds before the structure began to rebound. The maximum time-step was calculated to be 0.1593 microseconds, the same as in the previous impact simulation, resulting in 25,126 cycles. The finite element analysis required approximately three CPU hours to complete on a contemporary engineering workstation, with one cycle taking approximately 0.4 seconds to compute.

The predicted response of the analytical cellular structure was evaluated by comparing the accelerations of the modeled rigid body OS to the experimental surrogate OS. The comparison of the acceleration data can be viewed in Figure 20. Both sets of acceleration data were passed through a 2,500 Hz low-pass filter to extract the fundamental acceleration pulse. The OS experimental acceleration peaks at 0.001 seconds with a value of 2,200 g's, and then levels off at approximately 1,500 g's for one millisecond before dropping off at 0.0025 seconds. The analytical acceleration data shows a peak value of approximately 1,600 g's, but maintains a nearly constant value of 1,400 g's over approximately two milliseconds of the impact. There

were differences in the data that can be attributed to the physical separation between the OS and the CV/cellular structure. Because of a slight gap between the OS and the cellular structure, there is a delay in the onset of acceleration for the physical OS. Additionally, the gap increased the peak value of the OS acceleration. These effects were not reflected in the finite element results since the gap between the OS and the CV/cellular structure was not modeled.

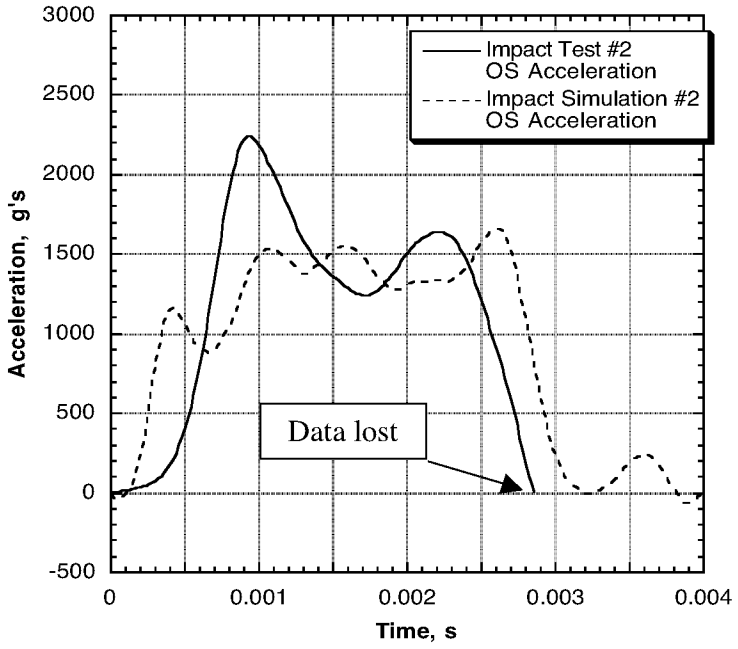

Figure 20 – Comparison of analytic and impact test acceleration for test #2.

The experimental velocity of the rigid body OS was calculated by integrating the experimental acceleration once. Figure 21 shows the comparison of the experimental velocity with the analytical velocity as determined by the finite element simulation. Excellent correlation was achieved between the analytical and test velocity data during the majority of the 0.004 second impact. The rebound velocity of the impact simulation was observed to be approximately

five meters per second. Although the experimental data was lost at approximately 0.003 seconds, the rebound velocity was estimated to be three meters per second by extrapolating the test data. Velocity data correlation was improved from impact simulation #1 and the results were judged acceptable. At the beginning of the impact, there was a slight discrepancy between the velocity distributions. This was due to a difference in the onset of OS acceleration between the analytical data and test data as observed in Figure 20.

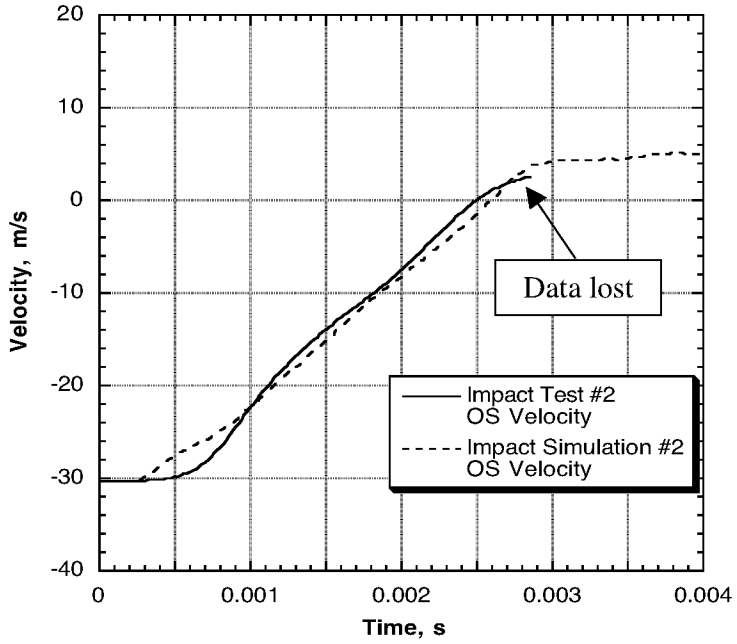

Figure 21 – Comparison of analytic and impact test velocity for test #2.

As with the velocity comparison, excellent correlation was achieved between the analytic and test data. The total crush stroke predicted by the analysis was 45 mm, or 65% of the available 69 mm crush distance. The simulation showed maximum crush occurred at approximately 0.0025 seconds into the impact. The numerical values closely matched the

experimental impact specimen, which had a crush stroke of 45 mm or 65% of the available crush distance. The displacement curve was determined by twice integrating the acceleration. Figure 22 shows a comparison of the analytic and experimental displacement of the OS rigid body. An image of the deformed cellular structure 0.003 seconds into the impact is shown in Figure 23.

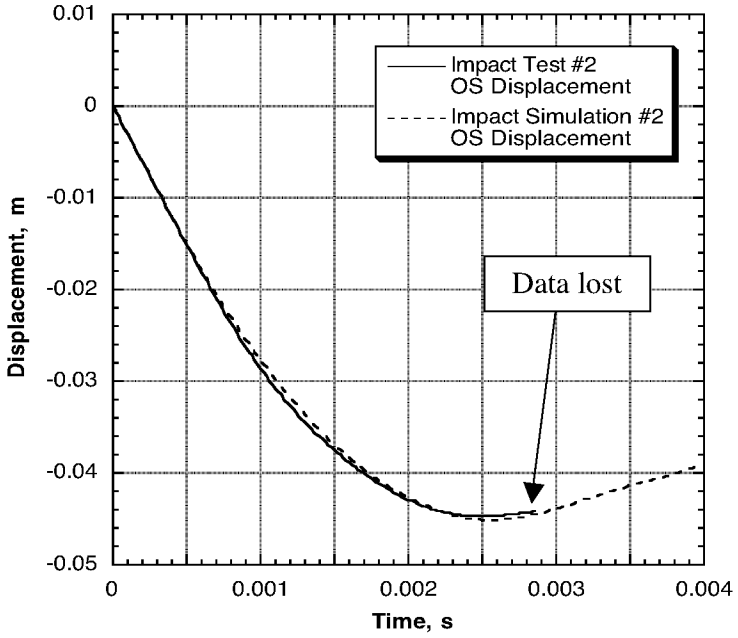

Figure 22 – Comparison of analytic and impact test displacement for test #2.

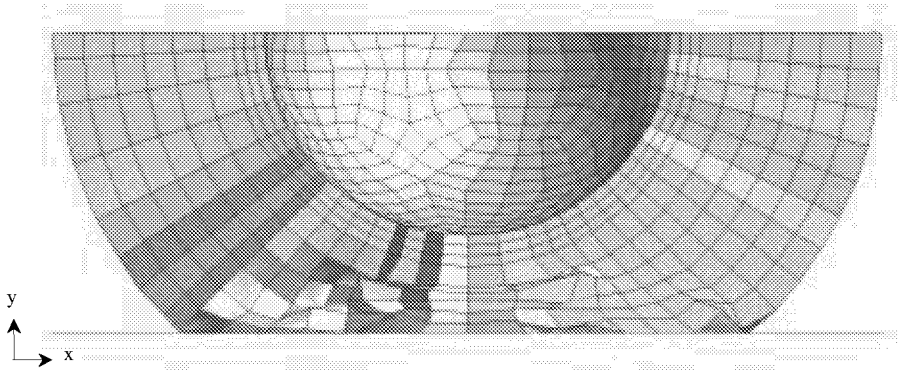

Figure 23 – Cross-section of deformed cellular structure #2, t = 0.003 s.

The comparison between experiment and analysis was considered acceptable based on good correlation between analytical and test data for the OS acceleration and excellent correlation of data for the OS displacement and velocity. For impact simulation #1, there was an excess of elastic energy in the system that generated a higher rebound velocity than observed in the test. Modeling the foam cores by using the FOAM1 material model with an effective Poisson's ratio of zero, decreased the amount of rebound velocity and elastic energy. With correlation between analytical and experimental data achieved, implementation of the FOAM1 material model seems to be justified and will be used in subsequent finite element simulations. However, this is only one option that was explored in modeling the second cellular structure.

9.0 Impact Simulation #3

The objective of the third impact test was to provide additional data to aid in the design of the cellular structure at higher impact speeds more representative of the EEV's terminal velocity. To achieve the higher impact velocity, a bungee accelerator was installed under the gantry, as shown in Figure 9. Using the bungee accelerator, the impact velocity of the third test specimen was 35.5 m/s. The impact test specimen was constructed using stronger, higher density polyurethane foam than previously used in the impact tests. Additionally, the thickness of the cell walls was increased to 3.05 mm, the same cell wall thickness used in impact test specimen #1. The cellular structure/retaining plate had a mass of 8.87 kg, and the orbiting sample (OS) had a mass of 3.51 kg, resulting in a total impact mass of 12.38 kg. The impact test specimen had an outside diameter of 0.314 m, including the layers of the Kevlar outer shell, and an inside diameter of 0.178 m, including the graphite inner shell. The thickness of the Kevlar plies that formed the CV was 5.6 mm. One accelerometer was located within the impact test

specimen to capture the OS acceleration response, while another accelerometer was mounted on the retaining plate to measure the cellular structure response, as shown in Figure 3. A low-g accelerometer was also used to determine the impact velocity. Digital video was used to capture the impact event. For the impact test, the OS acceleration was lost due to a failure in the accelerometer-umbilical connection. The acceleration of the plate was captured over the first 0.0025 seconds, before that cable was also severed.

9.1 Finite Element Model #3

Additional changes were made to the baseline finite element model to represent the physical changes made to the impact test specimen from previous tests. Otherwise, model discretization was unchanged. The material model for the polyurethane foam was updated to reflect the increased density and strength of the foam. As in the previous model, the polyurethane foam was modeled using the FOAM1 material model with a user defined stress-strain curve. The bulk modulus K of the new foam was 8.21 $x10^6$ Pa, the density was 111.5 kg/m^3, and the yield stress was 1.32 $x10^6$ Pa. As with the previous material model, the foam was defined to have an increase in stress due to compaction after approximately 90% strain.

The material model used for the hybrid composite cell walls was also updated to more accurately reflect the increased crushing that occurred in test #3. This was due to a greater amount of impact energy resulting from a higher impact velocity and increased mass. Accordingly, a larger amount of deformation was experienced; thus, the material model of the cell walls was modified to include a failure criterion. The failure model for the cell wall finite elements was based on a maximum plastic strain of 20%. Thus, the cell wall elements would fail once a plastic strain of 20% was reached. The failure value of plastic strain was determined

empirically by a parametric impact study of the cellular structure in which the analytical dynamic response was compared to the test dynamic response [20]. Using this method, 20% failure strain provided the best correlation.

For the third impact test specimen, the overall mass was increased when compared to the previous impact tests. Accordingly, each lumped mass was defined as 0.214 kg, resulting in a total amount of 6.42 kg added around the top of the model.

9.2 Numerical Results for Impact Simulation #3

The impact simulation was executed for 0.004 seconds, with rebound occurring at approximately 0.003 seconds. The maximum time-step for simulation #3 was 0.1593 microseconds and there were 25,126 cycles. A total run time of approximately three CPU hours on a contemporary engineering workstation was required for the simulation resulting in one cycle computed approximately every 0.4 seconds.

Since the OS acceleration was lost, the measured acceleration response of the plate was plotted and compared with analytical results from the finite element simulation in Figure 24. The acceleration data was filtered with a 5,000 Hz low-pass filter to extract the fundamental acceleration pulse. The difference in shape of the acceleration pulse when compared to the previous two simulations highlights the difference in the OS response versus the plate response. The plate acceleration data is noisier and has higher frequencies in the signal than observed in the OS data. When comparing the acceleration data from the test and simulation, the analytical acceleration data has an average value of approximately 1,650 g's while the experimental acceleration data has an average value of approximately 1,550 g's. When evaluating the peak acceleration of the cellular structure, the simulation calculated a maximum acceleration of

approximately 2,600 g's, while the peak acceleration measured during the impact test was also 2,600 g's. It is also observed that the overall average dynamic response of both acceleration curves gradually slopes upward. Although the test data ends at approximately 0.0025 seconds, the simulation was carried out to show the predicted response of the cellular structure through rebound.

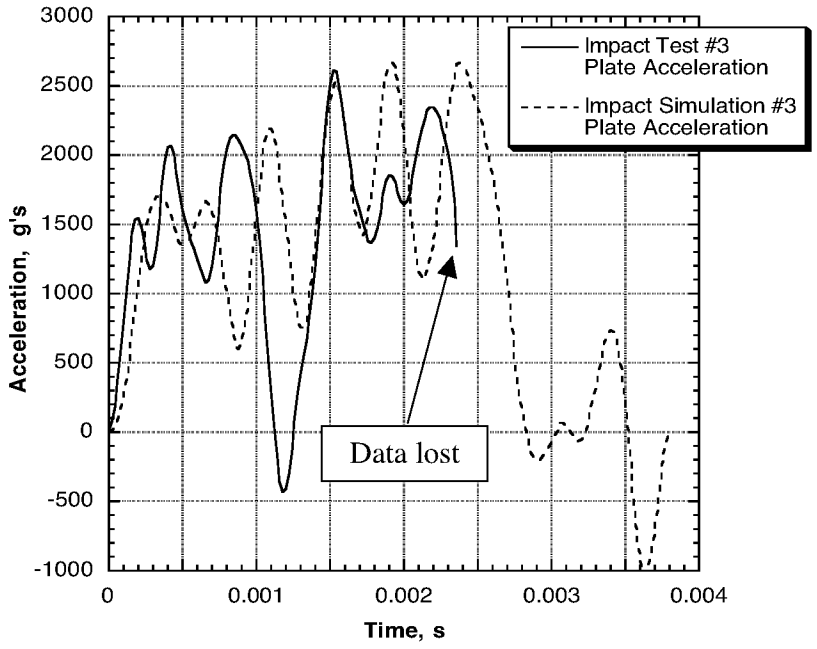

Figure 24 – Comparison of analytic and impact test acceleration for test #3.

The cellular structure velocity time-distributions, as determined by the finite element simulation and by integration of the impact test acceleration data, are shown in Figure 25. Excellent correlation was achieved between the available test data and the analytical data. An average rebound velocity of seven meters per second was predicted by the impact simulation. This value was slightly higher than the rebound velocity predicted in the previous simulation, but

with the increased impact velocity and greater mass, this result was determined to be acceptable. Additionally, the previous two impact simulations have slightly over-predicted the rebound velocity. Consequentially, the rebound velocity of the physical test specimen would be less than the predicted seven meters per second rebound velocity.

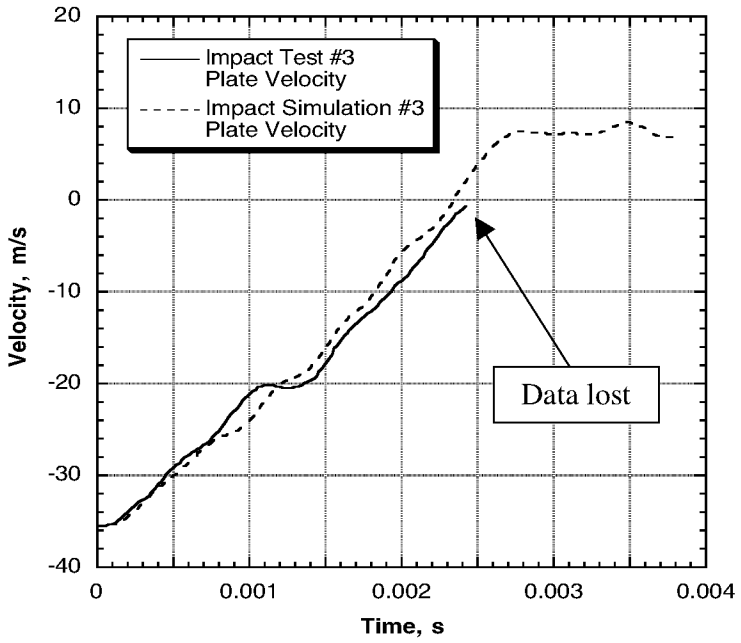

Figure 25 – Comparison of analytic and impact test velocity for test #3.

The total crush stroke predicted by the analysis was 54 mm, or 79% of the available crush distance. The simulation showed that maximum crush occurred at approximately 0.0025 seconds into the impact. As noted, acceleration test data was lost at the approximate time of maximum crush. However, by twice integrating the experimental acceleration, an estimate of the cellular structure crush stroke was obtained. Using this estimation, the impact specimen had a crush stroke of approximately 49 mm, or 72% of the available stroke. Figure 26 shows the analytical

and experimental variation in displacement. After the test, the crush stroke was estimated to be 79% of the available crush distance, 54 mm. The predicted crush stroke matched the post-test crush estimate and was 7% greater than the test data estimate. However, since the test data was not obtained through the full impact pulse, the post-test deformation pattern is likely a better estimate of the total stroke. Deformation of the cellular structure as predicted by the finite element simulation 0.003 seconds into the impact is shown in Figure 27. A photograph of the impact test specimen, which was bisected to allow for the observation of cell wall deformation, is shown in Figure 28.

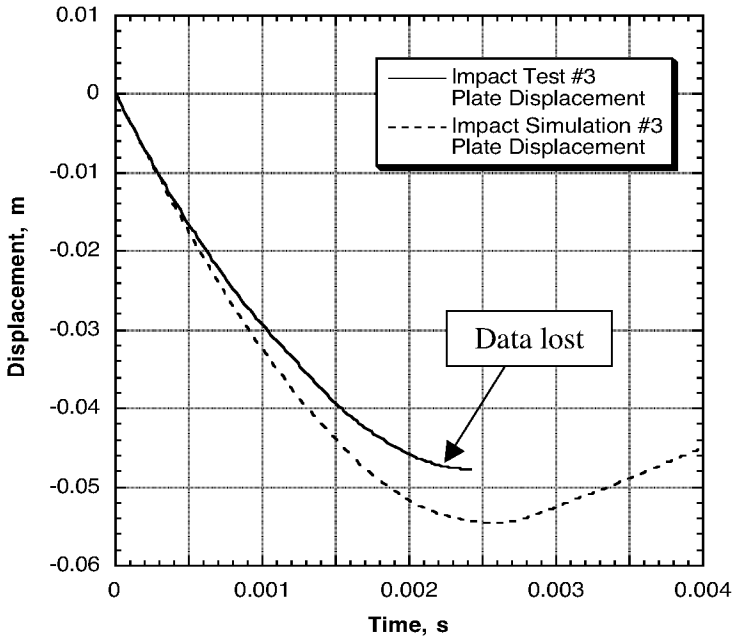

Figure 26 – Comparison of analytic and impact test displacement for test #3.

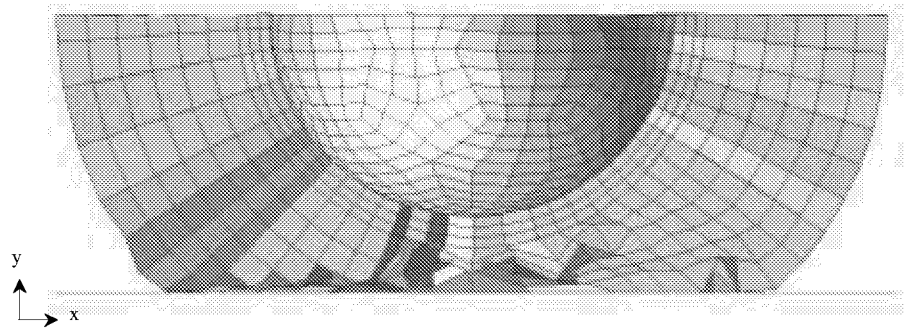

Figure 27 – Cross-section of deformed cellular structure #3, t = 0.003 s.

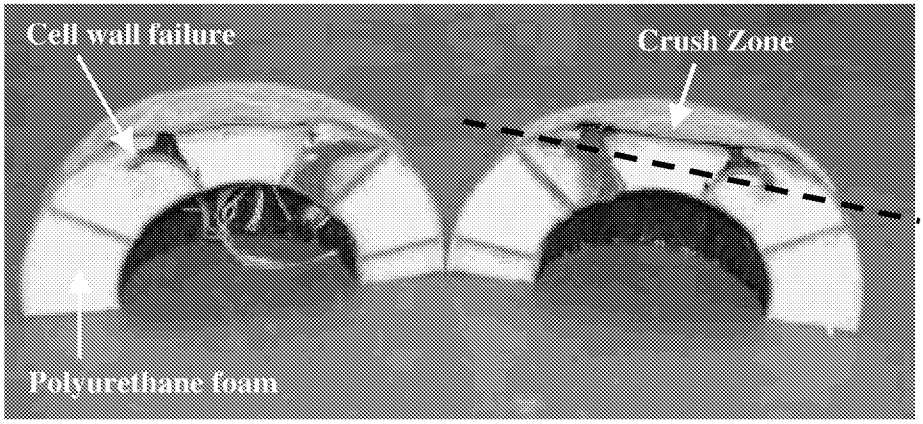

Figure 28 – Photograph of bisected cellular structure, after impact test #3.

Modifications to the finite element model proved to be beneficial in correlating the analytical response of the cellular structure to the test data. Both the average and peak acceleration values showed good correlation between test and simulation data. The velocity and displacement also matched up well when compared to test data. Modeling of the cell walls with a plastic strain failure criterion was determined to be acceptable and was used in subsequent simulations. By defining a plastic failure strain in the cell walls, in conjunction with using the FOAM1 material model, the increased amount of energy for test #3 was absorbed by the cellular structure in the simulation.

10.0 Impact Simulation #4

The fourth impact test specimen included a spherical shaped, full scale OS with an internal data acquisition system. Hardware representing the OS was delivered from NASA's Jet Propulsion Laboratory (JPL) for insertion into the cellular structure. The OS was aluminum, had an outside diameter of 0.155 m, and had a mass of 3.77 kg. The cellular structure had an outside diameter of 0.308 m, an inside diameter of 0.171 m, and a mass of 10.54 kg. This resulted in a total impact mass of 14.31 kg. The compressed thickness of the CV was approximately 4.8 mm and was used to fill an eight-millimeter gap between the OS and the cellular structure.

To achieve an impact speed representative of the expected vehicle terminal velocity, additional and stiffer bungee cords were used in the bungee accelerator. This change allowed for the impact velocity of the impact test specimen to be 40.4 m/s, which was determined after the test by a low-g accelerometer. One accelerometer was mounted on top of the OS to capture the OS acceleration data and two accelerometers were located on the retaining plate to measure the plate acceleration as shown in Figure 4. There was also a JPL supplied accelerometer located within the OS at the approximate center of mass. Digital video was used to capture the test.

In the fourth impact test specimen, the polyurethane foam cores were replaced with carbon foam cores, which will be used in the flight vehicle. Carbon foam is better suited for space applications due to low out-gassing, a higher stiffness to weight ratio, and structural integrity at higher reentry temperatures. The amount of Kevlar wrapped around the outside of the cellular structure was increased to 1.75 mm. The graphite-epoxy laminate that lined the inner surface of the cellular structure was also increased in thickness to 2.34 mm. Additionally, the thickness of the cell walls was increased by adding additional layers of graphite-epoxy and Kevlar, providing a cell wall thickness of 4.75 mm.

10.1 Finite Element Model #4

A more detailed finite element model was generated to represent the impact test specimen used in test #4. The cellular structure and impact surface were geometrically modeled in the same manner as the previous impact specimens, except as noted. The polyurethane foam was replaced with carbon foam and modeled with a FOAM1 material model. A piecewise linear stress-strain curve for the carbon foam was constructed using crush test data provided from penetration tests [5]. The 4-node shell elements that represented the graphite-epoxy/Kevlar cell walls, the graphite-epoxy inner surface, and the Kevlar outer surface were changed in thickness to match the physical test article.

In addition to these modified components, a spherical OS was geometrically discretized and replaced the hemispherical rigid body used in previous models to represent the OS. The retaining plate was also geometrically discretized and replaced the concentrated masses previously used in the finite element models. Both components were added to the baseline finite element model to match the geometry of impact test specimen #4. The finite element model of impact specimen #4 is shown in Figure 29. An exploded view of the finite element model is shown in Figure 30.

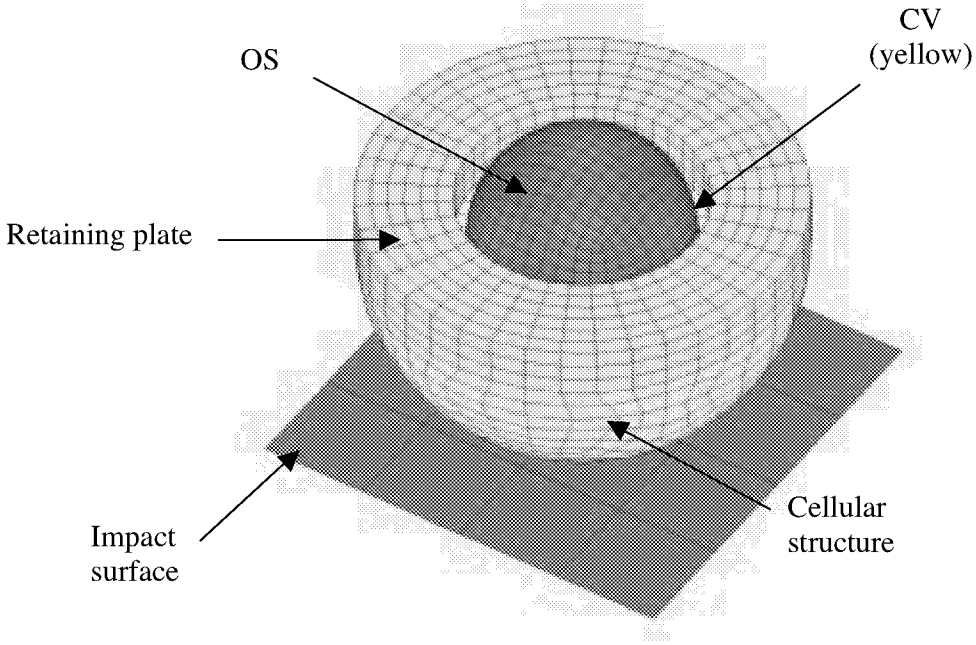

Figure 29 – Components of finite element model #4.

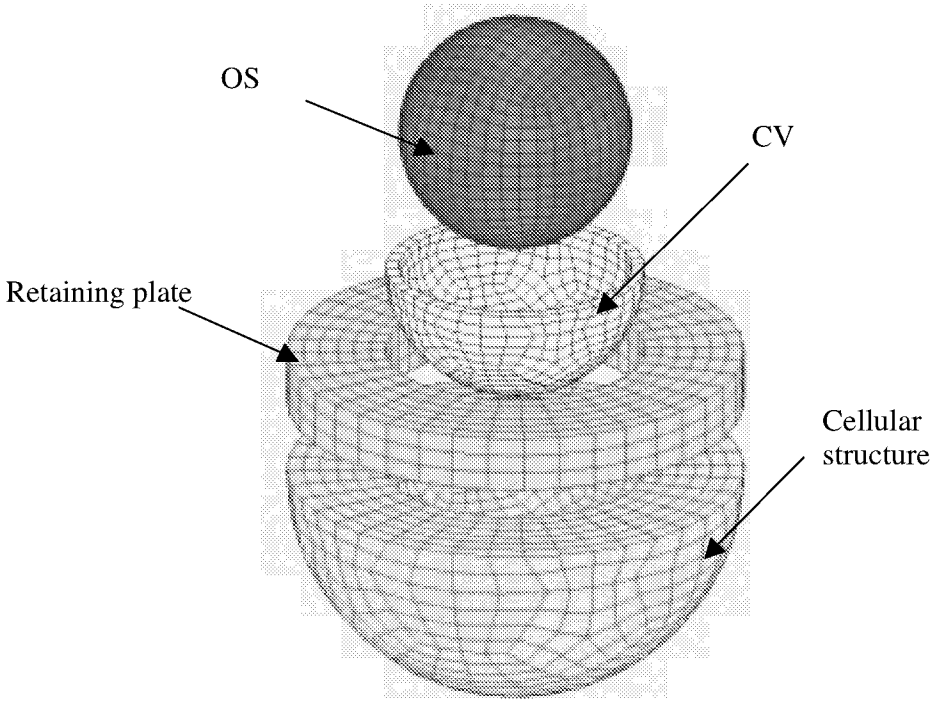

Figure 30 – Exploded view of finite element model #4.

The orbiting sample (OS) was modeled using 3,560 elements. The majority of the aluminum OS was modeled with 8-node, single integration point, Lagrangian solid elements. The material model for these elements was an isotropic, elastic-plastic material model. The remaining elements were used to model the inner surface of the OS and were defined as a rigid body. These elements were created to provide consistent output from the finite element simulation and to show the OS dynamic loads. To match the total mass of the physical OS, the rigid shells that lined the inner surface were defined to have an appropriate value, resulting in an OS analytical mass of 3.77 kg. Also, defined on the rigid body material card was the 40.4 m/s impact velocity for this test.

The back retaining plate was modeled using 8-node Lagrangian solid elements. An isotropic material model was used to define the retaining plate. For this impact test, the mass added to the cellular structure was 7.71 kg, which resulted in a retaining plate density of 3,852 kg/m^3.

Another update to the finite element model was to modify the containment vessel (CV) discretization. In previous impact simulations, the CV was modeled with three elements through the thickness. This required a small time-step due to the small elements in the CV. A study was performed to determine how the dynamic loads applied to the OS would change if the CV were modeled with one element through the thickness. The results showed that there was minimal change in the OS acceleration when the CV was modeled with one element through the thickness as compared with three elements. Accordingly, the CV was defined with one layer of 8-node brick elements and an elastic-plastic material model. In the same manner as for previous impact models, nodes on the bottom surface of the CV were equivalenced with nodes on the inner

surface of the cellular structure, effectively holding the CV in place. The same material properties were used to define the CV as in the previous impact models.

In previous models, the OS was represented by rigid body shells that lined the inner surface of the CV and was attached to the CV. With the OS geometrically modeled, the interaction between the CV (and cellular structure) and OS had to be defined. This boundary was defined by a contact surface between the OS and CV to ensure the OS would not go through the CV upon impact. In addition, nodes of the OS and CV were equivalenced to effectively hold the OS inside the cellular structure upon impact. The equivalenced nodes were located around the equator of the OS and on the top, inside surface of the CV.

Figure 31 shows the cross-section of the finite element model used for the fourth impact simulation. A summary of the material properties used in the finite element model for impact simulation #4 can be found in Table 3.

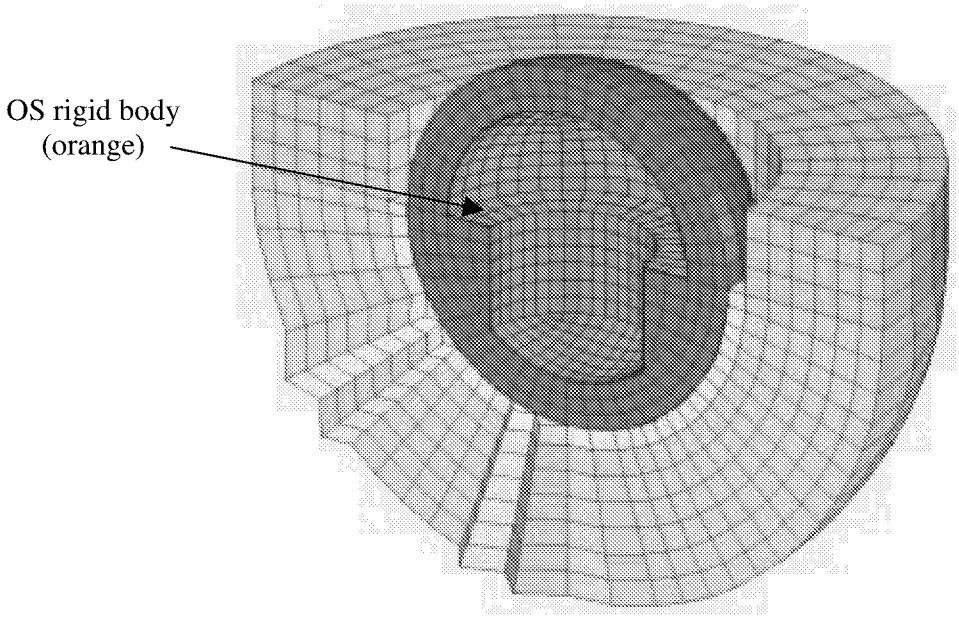

Figure 31 – Cross-section of finite element model #4.

Table 3 – Material property values used in finite element #4.

Material	Property Model	Material Model	Number of Elements	Density (kg/m^3)	Volume (m^3)	Mass (kg)
Cell Foam	PSOLID	FOAM1*	2,640	91.26	6.61×10^{-3}	0.60
Cell Walls	PSHELL	DYMAT24	1,320	1,539	9.78×10^{-4}	1.51
Inner Shell	PSHELL	DYMAT24	440	1,550	1.16×10^{-4}	0.18
Outer Shell	PSHELL	DYMAT24	440	1,379	2.71×10^{-4}	0.37
CV	PSOLID	DYMAT24	440	383	3.98×10^{-4}	0.15
OS	PSOLID	DYMAT24	2,720	1,947	1.43×10^{-3}	2.78
OS Rigid	PSHELL	MATRIG	840	N/A	N/A	1.00
Back Plate	PSOLID	DYMAT24	720	3,852	2.00×10^{-3}	7.71
Concentrated Masses			8	N/A	N/A	0.012
Total Number of Elements			**9,568**	**Total Impact Mass**		**14.31**

* Cell Foam modeled with user defined, bilinear, stress-strain curve

Table 3 (continued)

Material	Young's Modulus ($\times 10^9$ Pa)	Poisson's Ratio	Yield Strength ($\times 10^6$ Pa)	Shell Thickness ($\times 10^{-3}$ m)
Cell Foam	0.10	0.0	1.00	N/A
Cell Walls	21.20	0.3	212	4.75
Inner Shell	45.50	0.3	579	2.34
Outer Shell	6.895	0.3	103	1.75
CV	70.00	0.3	34.4	N/A
OS	68.95	0.3	689.5	N/A
OS Rigid	N/A	N/A	N/A	5.00
Back Plate	27.20	0.3	268	N/A

An additional method for constraining the OS in the cellular structure was also developed in which two contact surfaces were defined for the OS. One contact surface was defined between the OS and the CV, as in the current simulation, while a second contact surface was defined between the OS and a modified retaining plate that enclosed the OS. Effectively, the second contact surface held the OS inside the cellular structure. The model provided accurate results when compared to the fourth impact test. However, it was judged that the current method

for restraining the OS in the cellular structure was acceptable and that the second contact surface did not provide more accurate results.

10.2 Two-Body Interaction between OS and Cellular Structure

Upon reduction of the acceleration data for impact test #4, significant portions of the acceleration curve were observed to have high-amplitude pulses. This phenomenon occurred because of the initially soft, nonlinear CV material, which couples the OS to the cellular structure as shown in Figure 4. To illustrate the point, the experimental accelerations of the OS and the retaining plate for test #4 are shown in Figure 32. Note that there was a time delay of approximately 0.0005 seconds from the beginning of the plate/cellular structure acceleration pulse to the initiation of the OS acceleration pulse. This delay was due to the highly nonlinear CV material, which filled the gap between the OS and the cellular structure. Due to the interaction of the OS and the cellular structure, a large spike developed in the OS acceleration data at 0.0012 seconds, indicating that the CV underneath the OS was fully compressed. A decrease in the plate/cellular structure acceleration was also observed at the same time due to action-reaction forces. At 0.0024 seconds, the OS acceleration again increased and was then forced in the opposite direction due to a large plate/cellular structure acceleration, which occurred 0.0026 seconds into the impact. The OS acceleration then began to oscillate, indicating repetitive contact between the OS-cellular structure and OS-retaining plate, but eventually reached equilibrium and settled to zero.

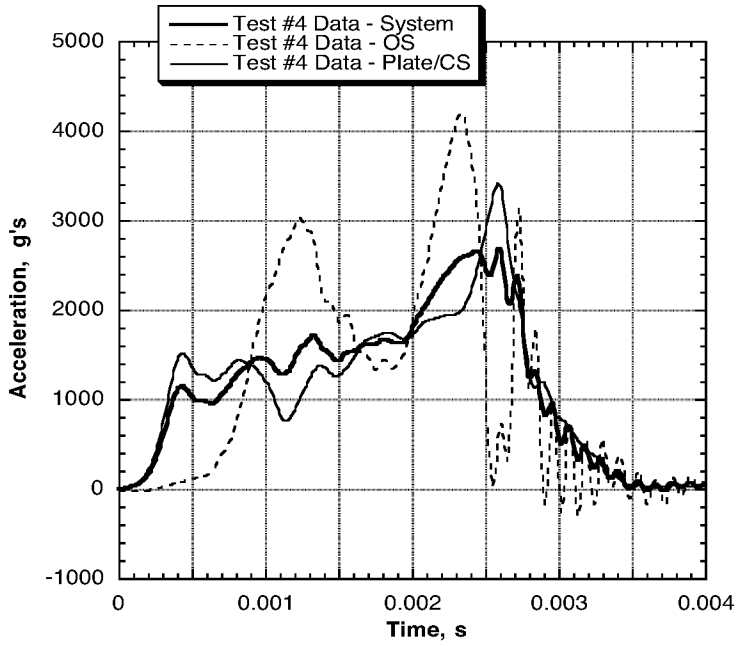

Figure 32 – Impact test #4 OS & plate/CS accelerations and equivalent system acceleration.

Consequently, to evaluate the dynamic response of the cellular structure and to remove the interaction between the two bodies during the impact, the following equation was developed [5, 20, 21].

$$F(t) = A_{CS}M_{CS} + A_{OS}M_{OS} = M_{TOTAL}A_{SYS} \quad \textbf{(1)}$$

Where F(t) is the crush force of the cellular structure, A_{CS} is the measured acceleration of the combined plate and cellular structure, A_{OS} is the measured acceleration of the OS, and A_{SYS} is the equivalent acceleration of the entire system (or the acceleration at the cm of the impact test specimen). Solving for the system acceleration:

$$A_{SYS} = (A_{CS}M_{CS} + A_{OS}M_{OS}) / M_{TOTAL} \quad \textbf{(2)}$$

For equation 2 to apply, the retaining plate must be rigidly attached to the cellular structure and the mass of the crushed portion of the sphere must be small compared with the total mass. By using the system acceleration, the peaks due to the two separate bodies were eliminated (see Figure 32), and a better representation of the behavior of the cellular structure for a "perfect CV coupling" is obtained. Consequently, to obtain the perfect coupling in the finite element model, the CV was equivalenced to the cellular structure, and the OS was then coupled to the cellular structure with equivalent nodes around the OS equator.

10.3 Numerical Results for Impact Simulation #4

The impact simulation was run for 0.004 seconds, which required 3.3 CPU hours on a contemporary engineering workstation. The maximum time-step for this model was 0.2018 microseconds, an increase of 27% from previous models resulting from the updated modeling of the CV. However, the actual run time was not substantially decreased due to additional elements in the finite element model. The simulation took 20,788 cycles to execute the simulation with each cycle taking approximately 0.6 seconds.

To make a meaningful dynamic comparison, the acceleration data was passed through a 1,000 Hz low-pass filter to extract the fundamental acceleration pulse. Both the analytical and experimental acceleration curves quickly rose to an average value of 1,500 g's where the curves gradually slope upward for 1.5 milliseconds. This is an indication of the sustained crush and energy absorption ability of the cellular structure. At approximately 0.002 seconds, the acceleration curves for both analysis and test rose to their peak values and were an indication of the cellular structure reaching maximum stroke. The finite element simulation predicted a peak system acceleration of 2,700 g's, which matched the experimental peak system acceleration.

After this time, both acceleration curves decreased as the cellular structure began to rebound. The general shape of the numerical acceleration pulse matched the experimental pulse, however the analytical acceleration dropped off slightly earlier than the experimental acceleration. Figure 33 shows the comparison of the two acceleration pulses.

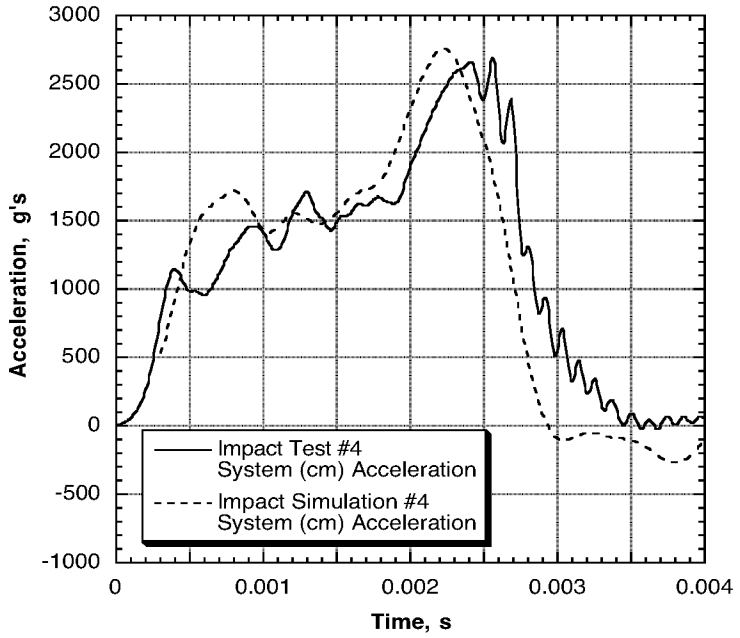

Figure 33 – Comparison of analytic and impact test acceleration for test #4.

For the fourth impact test, the velocity at the cm of the cellular structure was determined by integrating the system acceleration data. This data was then compared to the velocity of the rigid OS and can be viewed in Figure 34. The simulation accurately predicted the velocity of the cellular structure through the first 0.0015 seconds. After that time, the analytical velocity decreases slightly faster than the test data. The rebound velocity of the analytical cellular structure was approximately six meters per second. This value compared favorably with the rebound velocity of the test specimen, which was approximately five meters per second.

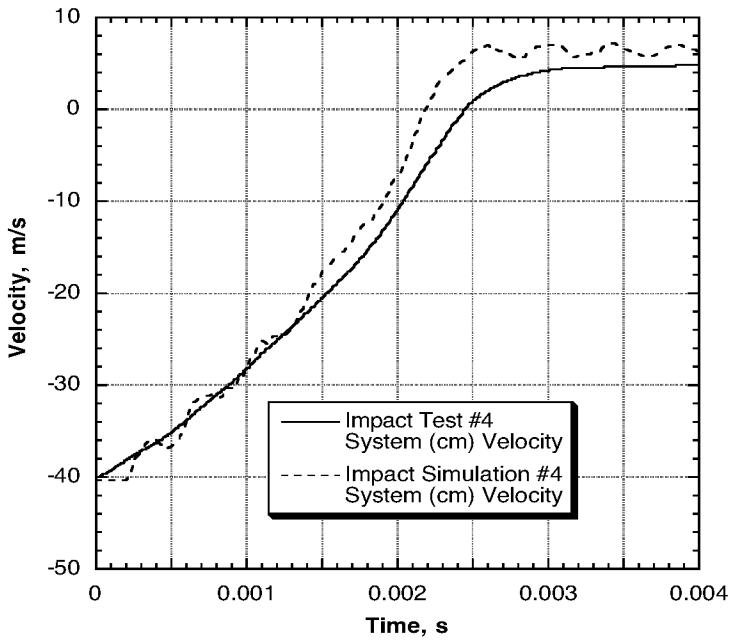

Figure 34 – Comparison of analytic and impact test velocity for test #4.

The variation in displacement of the experimental specimen was determined by twice integrating the acceleration data. Figure 35 shows the comparison of the analytical displacement with the experimental displacement. The overall crush stroke of the cellular structure as determined by the finite element simulation was 55 mm, or 81% of the available 68 mm crush stroke. This compares favorably with the impact test results, which indicated a crush of approximately 58 mm, or 85% of the available crush distance. A deformed plot of the finite element model showing maximum crush is shown in Figure 36, and a post-test photograph of the bisected impact test specimen is shown in Figure 37.

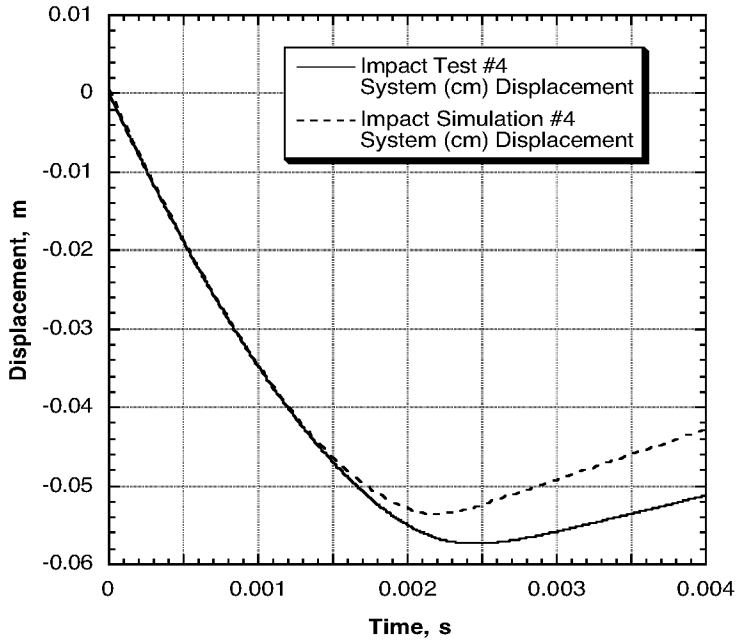

Figure 35 – Comparison of analytic and impact test displacement for test #4.

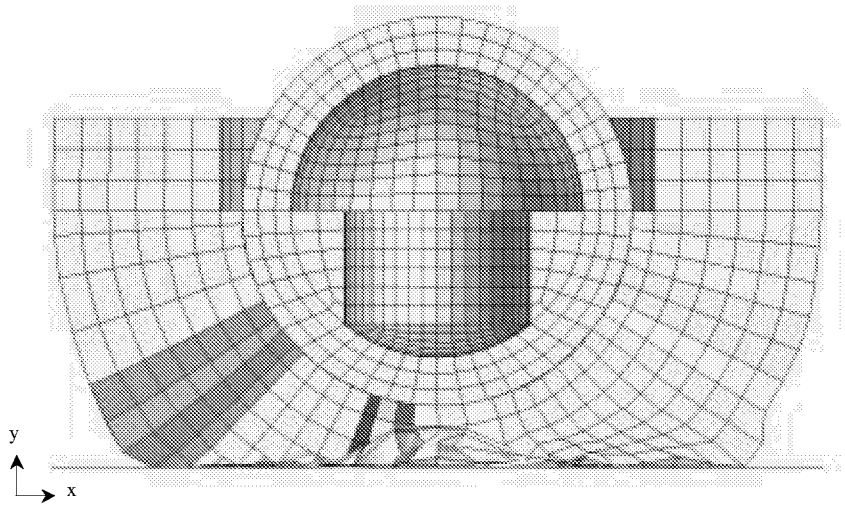

Figure 36 – Cross-section of deformed cellular structure #4, t = 0.002 s.

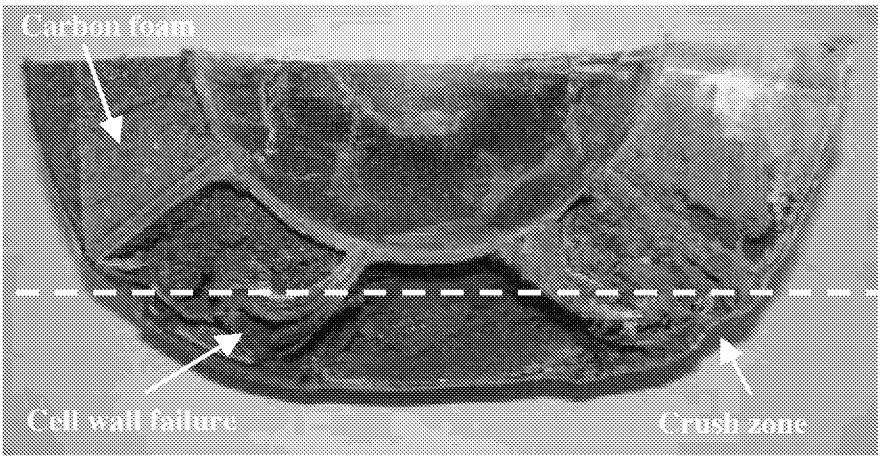

Figure 37 – Photograph of bisected cellular structure, after impact test #4.

The more detailed impact test specimen, and corresponding finite element model, proved challenging to predict the dynamic response of the cellular structure. The inclusion of the OS into the cellular structure, and the resulting two-body interaction further complicated the data analysis. By using the FOAM1 material model for the foam cores, defining a failure strain for the cell walls, and appropriately modeling the OS/CV interface, the appropriate combination of parameters were applied to accurately predict the acceleration, velocity, and displacement of the cellular structure.

11.0 Off-Nominal Impact Simulations

With correlation of the dynamic model achieved for four impact tests, analyses could be performed to determine how the cellular structure would respond to various impact surfaces with confidence. The finite element model described for impact simulation #4 was used for the off-nominal impact simulations. One off-nominal simulation was obtained by rotating the cellular structure 20 degrees to cause the impact point to occur at the intersection of a cell wall. Another

simulated off-nominal impact condition was to impact the cellular structure on an angled surface, again at a web intersection. Finally, the last off-nominal impact simulation describes how the cellular structure would respond to an impact on a corner.

11.1 Impact Simulation of Rotated Cellular Structure

One of the most probable off-nominal impact cases is one in which the cellular structure impacts a flat surface with a rotation angle. In the four impact tests conducted at the IDRF, the impact rotation ranged between two and 11 degrees. To present an extreme case, the cellular structure impact model was rotated 20 degrees with an impact velocity normal to the surface. This corresponds with the cellular structure hitting directly on a web intersection, the stiffest area of the cellular structure. Figure 38 shows a cross-section of the dynamic finite element model used in the simulation. The velocity for this impact simulation was 40 m/s in the negative y-direction and is normal to the impact surface.

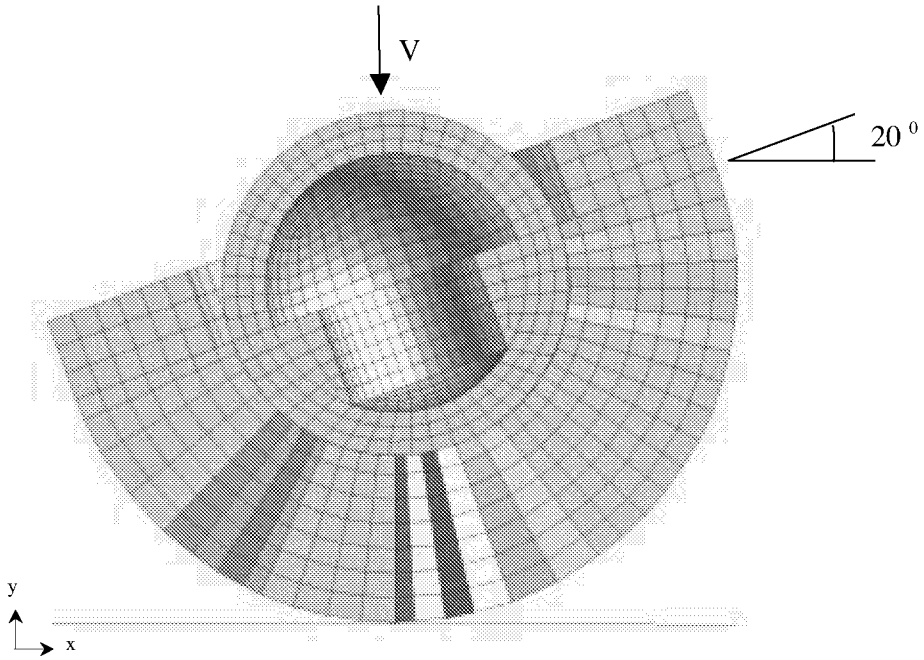

Figure 38 – Rotated cellular structure finite element model.

11.2 Numerical Results and Discussion of Rotated Cellular Structure

The simulation of the rotated cellular structure into the rigid surface produced results that were qualitatively intuitive. For the off-nominal impact, the simulation was run for 0.006 seconds to ensure the complete acceleration pulse was captured. However, when looking at the data, the cellular structure rebounds before 0.004 seconds, similar to the previous simulations. The simulation took 29,740 cycles and 4.6 CPU hours to complete on a contemporary engineering workstation with each cycle taking approximately 0.6 seconds to compute.

With the impact of the cellular structure on a web intersection, the peak acceleration of the cellular structure was greater that when there was no angle of rotation. This is intuitive as the web intersection is a stiffer area of the cellular structure and would deform less than if the impact occurred at the middle of a cell. To extract the fundamental acceleration pulse, the data was passed through a 1,000 Hz low-pass filter. A nearly symmetric impact pulse is observed in the acceleration data with a peak value reached in 0.0015 seconds, which then drops off to approximately zero by 0.003 seconds. The filtered acceleration data from the impact simulation shows a peak value of approximately 3,600 g's, which is slightly higher than the containment assurance limit of 3,500 g's. However, the dynamic loads on the cellular structure were only above the acceleration limit for approximately half a millisecond. The acceleration of the rotated cellular structure is shown in Figure 39.

The rebound velocity of the cellular structure was similar to what was observed in previous impact simulations. The cellular structure rebounded off the impact surface by 0.003 seconds with a velocity of approximately six meters per second, which corresponds to a maximum rebound height of 1.8 meters. Figure 40 shows the variation in velocity of the cellular structure as determined by the impact simulation.

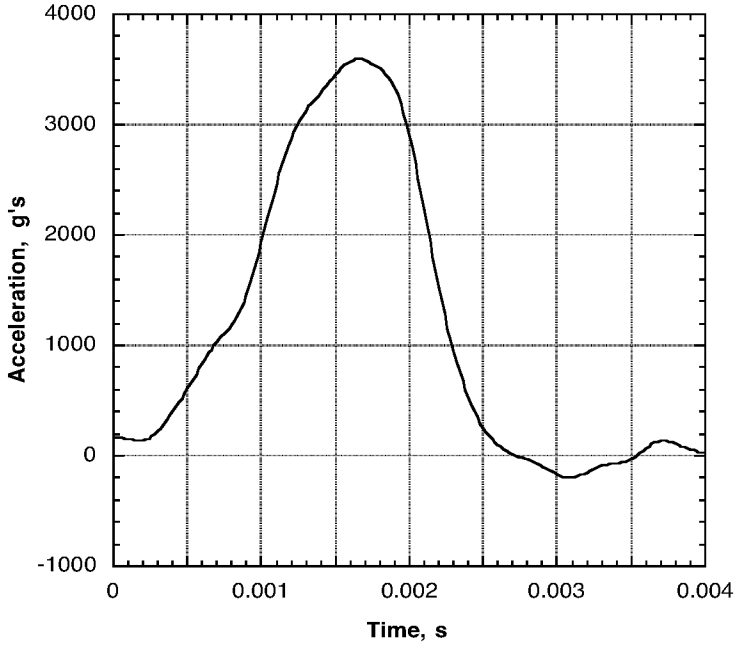

Figure 39 – System (cm) acceleration of rotated cellular structure.

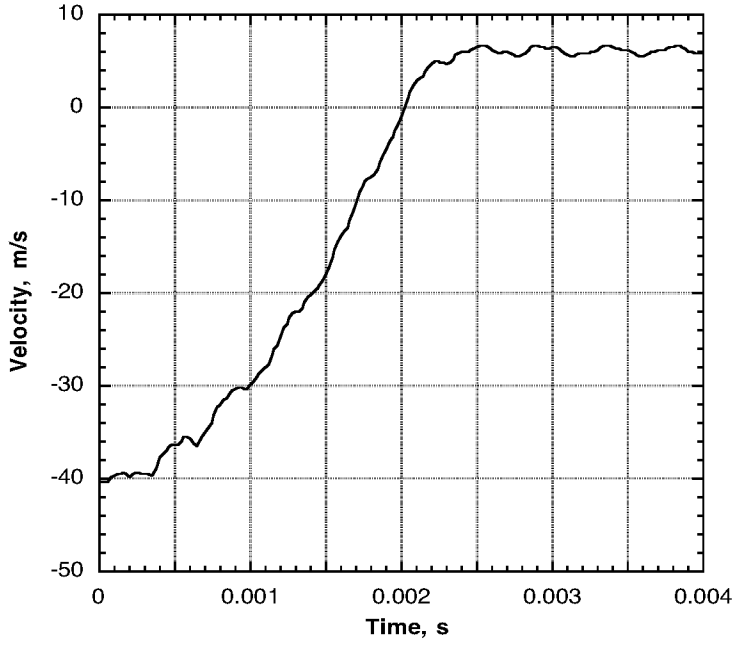

Figure 40 – System (cm) velocity of rotated cellular structure

A crush stroke of 52 mm, or 76% of the available crush stroke was observed when the cellular structure impacted at a web intersection. The amount of crush stroke is slightly less than observed in the previous simulations. Again, this is intuitive, as the cellular structure impacts at a web intersection, which offers more deformation resistance than the middle of a cell. Figure 41 shows the variation in displacement of the cellular structure and Figure 42 shows the cellular structure at maximum deformation.

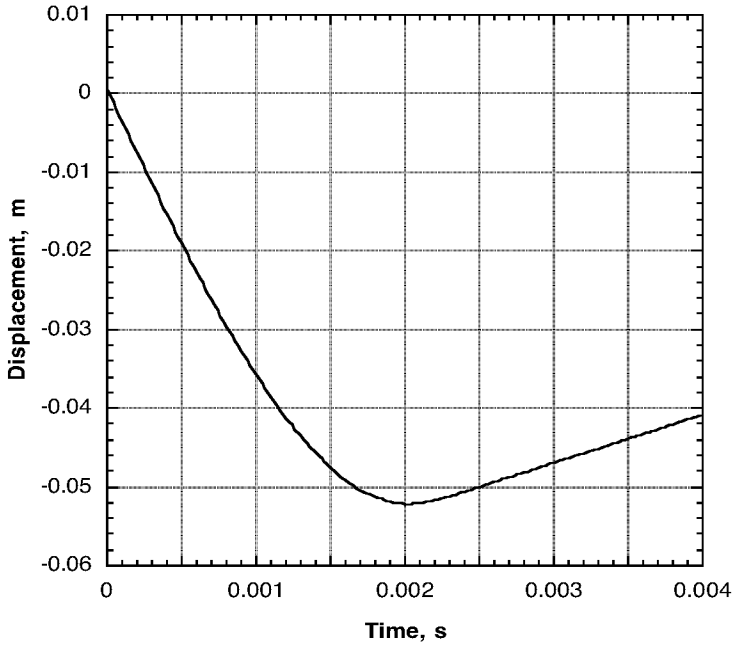

Figure 41 – System (cm) displacement of rotated cellular structure

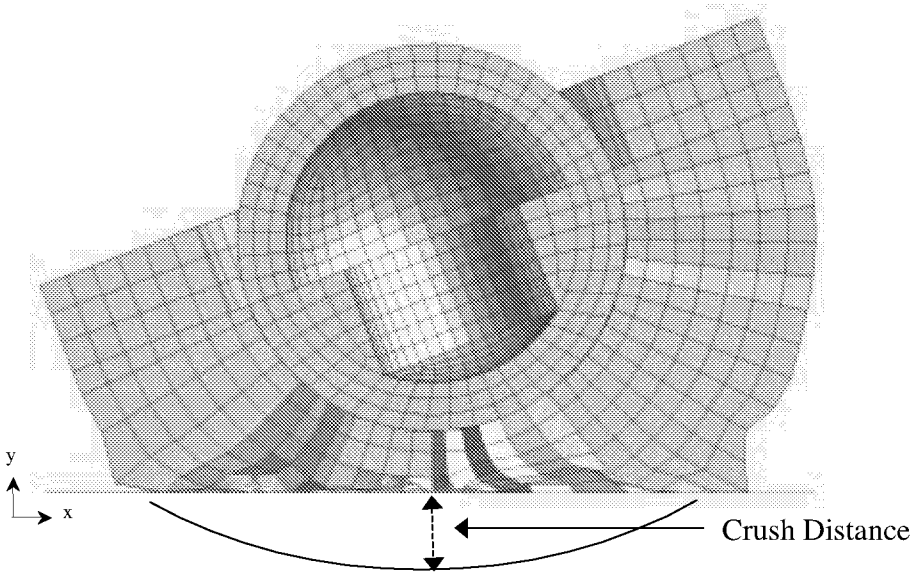

Figure 42 – Cross-section of deformed, rotated cellular structure, t = 0.002 s.

The dynamic response of a 20 degree rotated impact test specimen provided insight into the performance of the cellular structure. The acceleration of the cellular structure briefly rose above the 3,500 g sample containment criterion, but for only a brief period. As observed in the four impact tests, the maximum impact rotation was 11 degrees. For these tests, the acceleration loads did not exceed the containment assurance limit. However, the analysis indicated that impact at a cell wall intersection may produce dynamic loads on the OS that could possibly exceed the containment assurance criterion. Further analyses should be performed to evaluate the dynamic response of the cellular structure at different impact rotations. Additionally, further analysis on cell wall materials, layup, or thickness could be performed to optimize the cell wall design. For the studied impact scenario, the cellular structure does not completely crush upon a hard surface impact simulation.

11.3 Impact Simulation of Cellular Structure into an Angled Surface

The targeted impact zone for the EEV is the Utah Test and Training Range (UTTR), an area in western Utah where the ground consists of soft clay soil. The dynamic loads associated with this type of nominal impact have been studied in reference [4]. However, there are a number of mountains, large rocks, and sloped surfaces surrounding the UTTR landing site. The probability of EEV landing outside the landing ellipse and into an angled surface can not be considered zero. With the cellular structure model correlated to dynamic loads, an impact simulation into an angled surface was performed.

Changes to the finite element model included moving the impact surface and modifying the cellular structure-impact surface contact definition. Again, to show an extreme case, the impact surface was rotated clockwise 20 degrees and moved such that the cellular structure would impact at a web intersection. A 0.4 coefficient of friction was defined in the contact algorithm to keep the cellular structure from sliding down a frictionless surface. This value was determined by an experiment between a flat sample of the Kevlar used on the outer surface of the cellular structure and the concrete surface at the IDRF. Figure 43 shows the cross-section of the dynamic finite element model used for this simulation. The velocity of this impact simulation was 40 m/s in the negative y-direction.

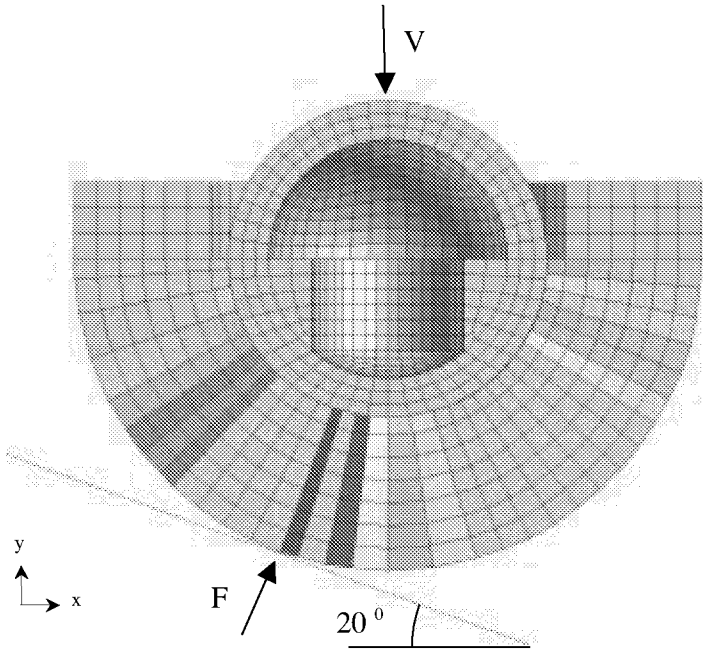

Figure 43 – Cellular structure finite element model, impact into an angled surface.

11.4 Numerical Results and Discussion of Cellular Structure into an Angled Surface

The simulation of the cellular structure impact sphere into an angled surface produced results in both the global x- and y-directions. The acceleration was reported as a magnitude to show the total dynamic load on the cellular structure during the impact. The velocity was reported as components in the global x-y coordinate system. Displacement values were reported in a transformed coordinate system relative to the impact surface to determine the amount of crush with respect to the impact surface. As with the previous case, the simulation was run for 0.006 seconds to ensure the dynamics of the problem were fully captured. However, the cellular structure rebounded off the impact surface within 0.004 seconds. The simulation took 5.5 CPU hours to run on a contemporary engineering workstation. It took 29,741 cycles to execute the simulation with each cycle taking approximately 0.7 seconds.

In the impact simulation, there were two components of acceleration. However, the design of the cellular structure lends itself to be able to absorb energy in all directions. Thus, the total acceleration observed by the cellular structure is of importance. The variation in acceleration magnitude, passed through a 1000 Hz low-pass filter, is shown in Figure 44. As determined from the impact simulation, the peak total acceleration on the cellular structure was 2,900 g's, which occurred approximately 0.0018 seconds into the impact event. The acceleration pulse duration was approximately 0.003 seconds and had a similar shape as observed in the rotated cellular structure impact simulation. It was noted that the acceleration began to level off at approximately 0.0008 seconds, indication of a possible cell wall failure. The acceleration then quickly rose to the peak value 0.001 seconds later, indicating the cellular structure was near maximum stroke.

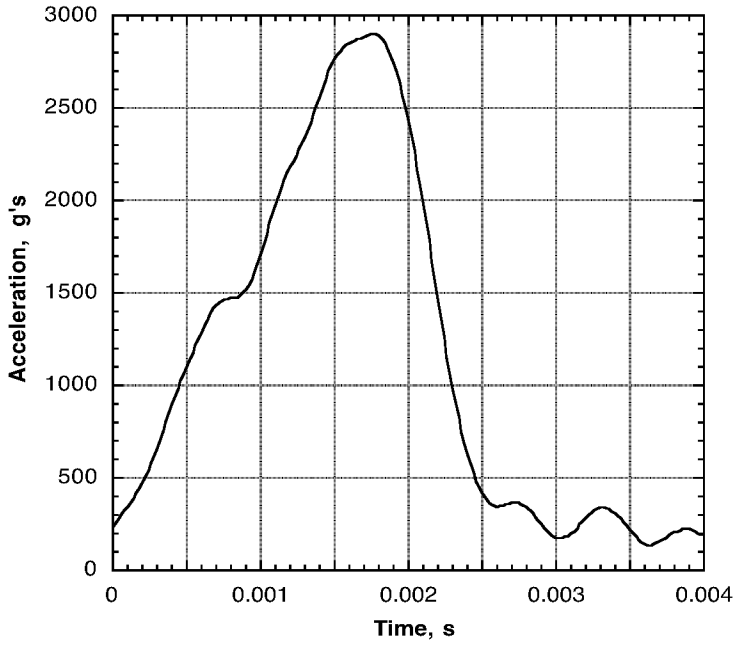

Figure 44 – System (cm) acceleration of cellular structure impact into an angled surface.

The velocity of the cellular structure during the impact simulation transitioned from a negative velocity in the y-direction to a positive velocity in both the x- and y-direction. This shift in direction is primarily due to the shape of the impact surface. The magnitude of the rebound velocity was approximately eleven meters per second, closely matching the rebound velocity in the x-direction, and higher than observed in previous simulations. The cellular structure was deflected horizontally and did not significantly rise after impact. However, the omni-directional design of the cellular structure was intended to provide protection for all orientations. Figure 45 shows the horizontal and vertical velocity of the cellular structure during the impact simulation.

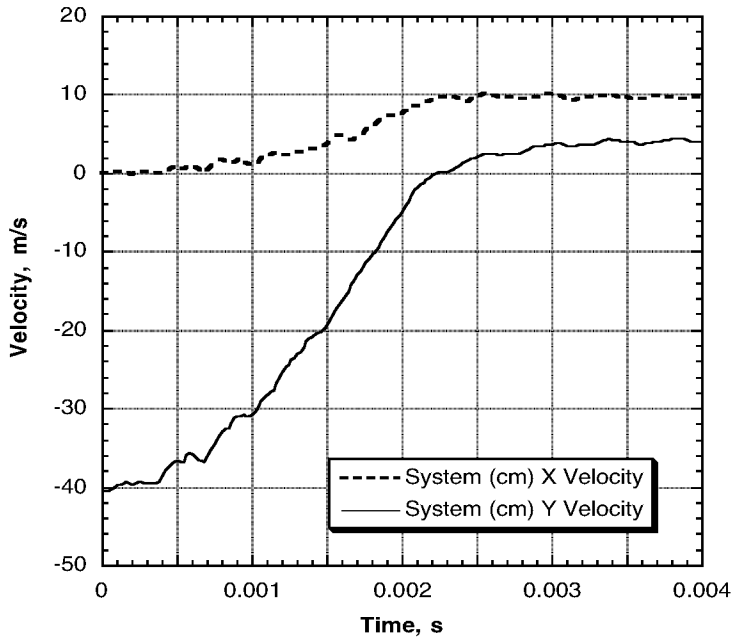

Figure 45 – System (cm) velocities of cellular structure impact into an angled surface.

The cellular structure crush distance was determined relative to the impact surface using components of displacement in the global x- and y-direction. The maximum value was observed to be 49 mm, or 72% of the available 68 mm crush stroke. The crush stroke for this type of impact was lower than observed in previous impact simulations and can be attributed to the cellular structure impacting at a web intersection and at an angle. Figure 46 shows the displacement of the OS rigid body, with respect to the impact surface, over time. Figure 47 shows the cellular structure at 0.002 seconds, when maximum deformation occurred.

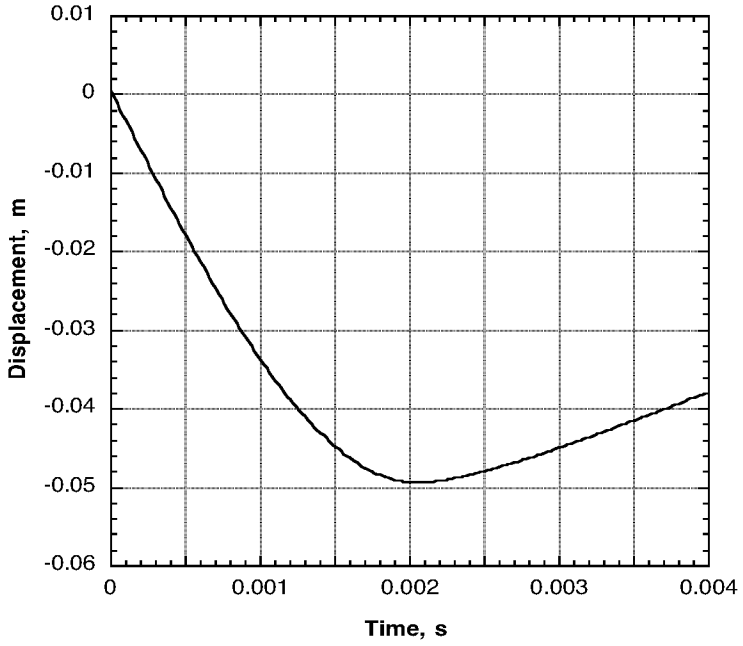

Figure 46 – System (cm) displacement of cellular structure impact into an angled surface.

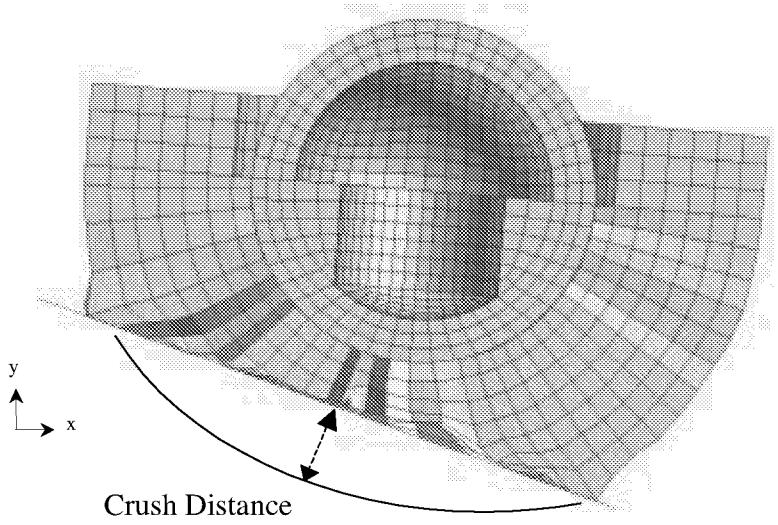

Figure 47 – Cross-section of deformed cellular structure into an angled surface, t = 0.002 s.

Impact simulations of the cellular structure into an angled surface show that the current energy-absorbing concept will perform as intended for this off-nominal impact case. Both the magnitude of the acceleration and the cellular structure crush distance were within the current limits set for containment assurance. Additionally, the rebound velocity was only slightly higher than previously observed and judged acceptable.

11.5 Impact Simulation of Cellular Structure into a Corner

The last off-nominal impact condition was to study the dynamic response of the cellular structure into the corner of a step. Included in the UTTR landing site are concrete slabs and other obstructions having corners. The probability of this type of impact can also not be considered zero. To simulate the impact of the cellular structure into this surface, a step with a height equal to half the cellular structure radius was modeled. The corner of the step was removed to eliminate numerical problems associated with a cellular structure impact into a sharp

corner. However, the elements that cut the corner were required to be larger than the elements on the bottom surface of the cellular structure to ensure the contact algorithm properly determined the contact forces. Additionally, the middle of cellular structure was positioned over the corner of the step. Figure 48 shows a cross-section of the dynamic finite element model used for this simulation. The velocity for this impact simulation was 40 m/s in the negative y-direction.

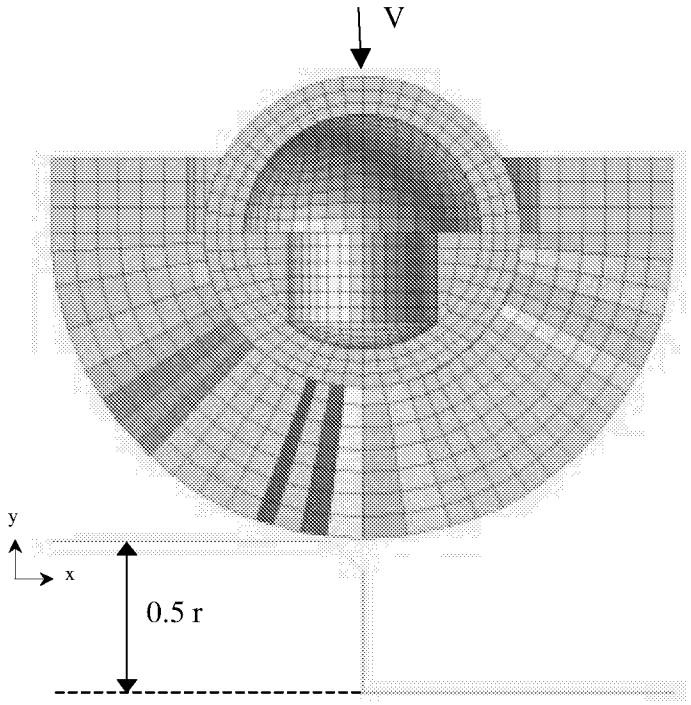

Figure 48 – Cellular structure finite element model, impact into a corner.

11.6 Numerical Results and Discussion of Cellular Structure into a Corner

The simulation of the cellular structure impact sphere into the corner of a step was run for 0.006 seconds to ensure the complete acceleration pulse was captured. This resulted in 29,786 cycles during the simulation. Again, the cellular structure rebounded off the surface within

0.004 seconds. The finite element simulation took 4.67 hours to complete on a contemporary engineering workstation with one cycle taking approximately 0.6 seconds to compute.

When the cellular structure impacted the corner of a step, only half of the structure was utilized to absorb the impact energy. Even under this severe condition, the simulation predicted that the cellular structure will absorb the impact energy and keep the dynamic loads to the OS under the 3,500 g containment assurance limit. The acceleration of the cellular structure impacting a corner was passed through a 1,000 Hz low-pass filter and can be viewed in Figure 49. The dynamic forces on the cellular structure rose to a value of 1,250 g's in less than a millisecond, but then decreased back to 800 g's, possibly indicating cell wall failure. The analytical acceleration then rose to a peak value of 2,200 g's at approximately 0.0023 seconds into the impact event, where the cellular structure has effectively bottomed out. When the cellular structure impacted the corner, nearly all the dynamic forces were in the vertical direction. As the simulation progressed, the cellular structure was observed to rotate around the corner and develop horizontal forces. However, the magnitude of the acceleration showed no appreciable change from the vertical component of acceleration. Only the vertical acceleration was presented and the horizontal component of acceleration was neglected.

The variation in velocity indicated that the cellular structure dynamically responded to a corner impact in a similar manner as to what was observed when the structure impacted an angled surface. While the vertical velocity decreased, there was an increase in the horizontal component, resulting in a total rebound velocity of eleven meters per second. The rebound was mainly in the horizontal direction and supported the observation that the structure will rotate around the corner. Figure 50 shows the velocity of the cellular structure as predicted by the impact simulation.

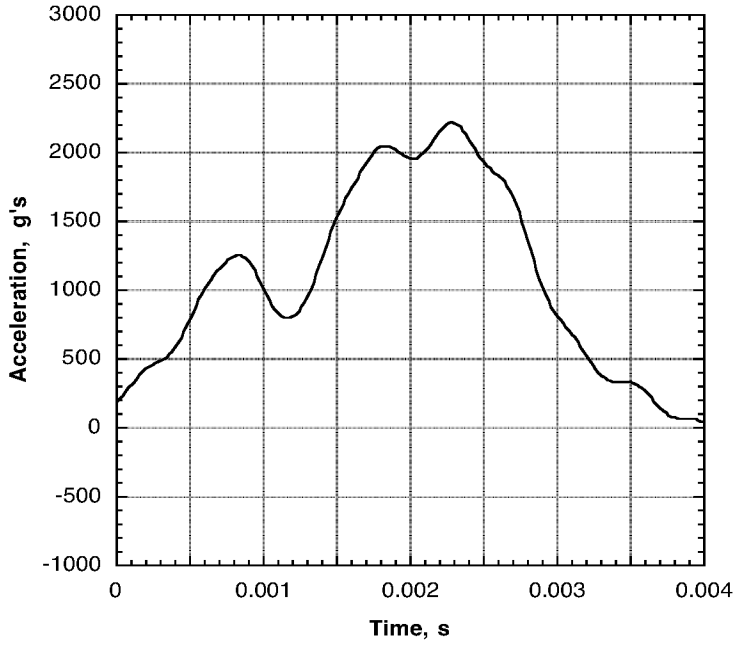

Figure 49 – System (cm) acceleration of cellular structure impact into a corner.

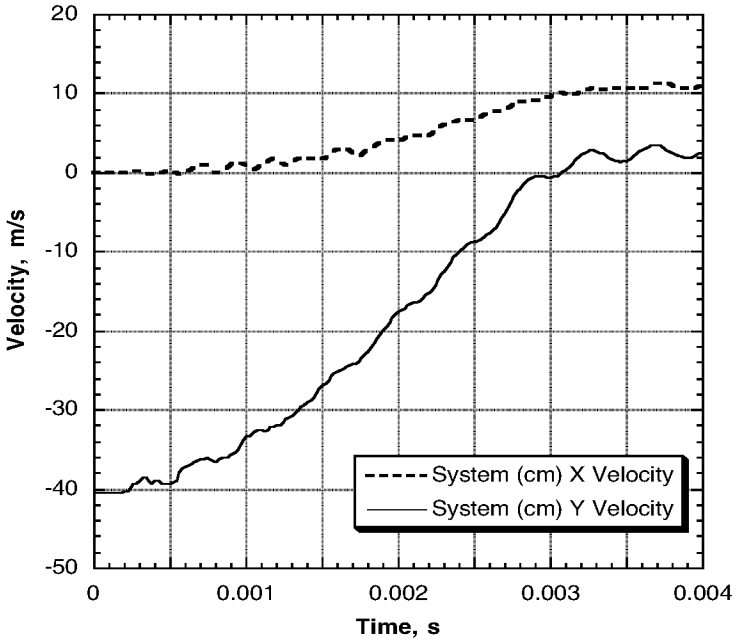

Figure 50 – System (cm) velocities of cellular structure impact into a corner.

Figure 51 shows the variation in displacement of the rigid body OS during the impact simulation. The displacement is referenced to a fixed location on the impact surface, which produced the crush indicated in Figure 52. The finite element simulation predicated that half the cellular structure would completely crush during impact into the corner. This can be observed in Figure 52, which shows the cellular structure at maximum deformation, which occurred at 0.003 seconds. The maximum crush was 68 mm, or 100% of the available crush distance. Of all the executed impact simulations, this model predicted the greatest amount of crush distance for the cellular structure. In Figure 52, the apparent impact surface penetration by the cellular structure, is an artifact of the model and post-processing of the simulation.

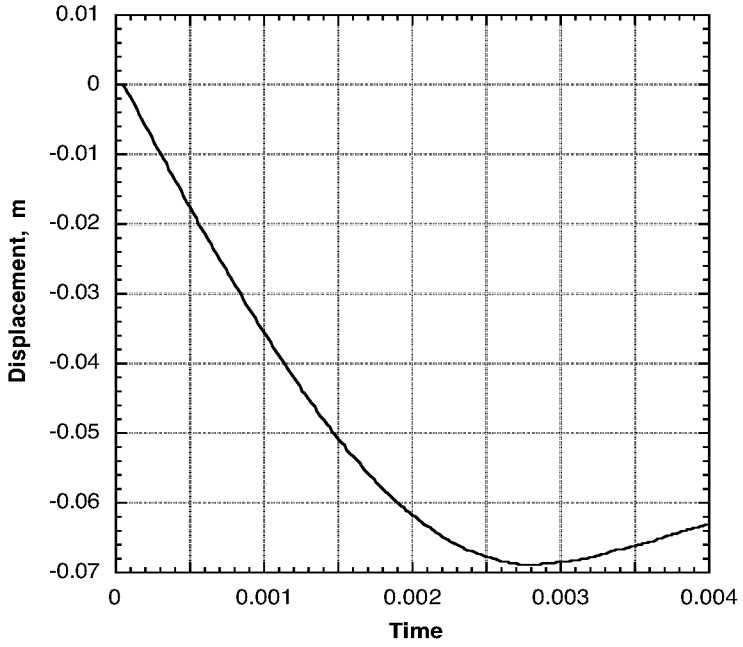

Figure 51 – System (cm) displacement of cellular structure impact into a corner.

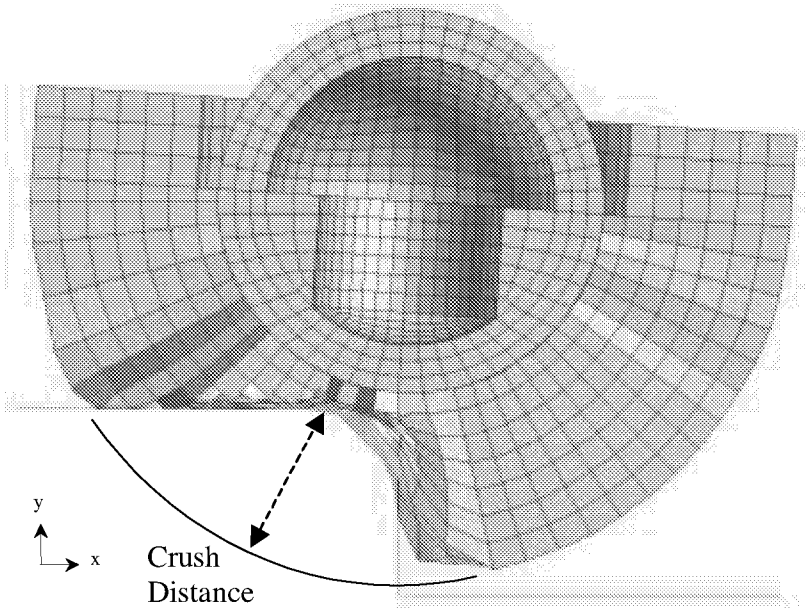

Figure 52 – Cross-section of deformed cellular structure into a corner, t = 0.003 s.

The impact simulation of the cellular structure into a corner showed that while the acceleration loads on the OS were predicted below the containment assurance limit, the impact sphere fully crushes at the corner. A potential containment problem could exist for this type of impact surface. To decrease the crush distance of the cellular structure, the thickness of the Kevlar outer shell could be increased to offer greater penetration resistance. Further analysis should be performed to optimize the cellular structure design for this type of impact.

12.0 Conclusions

Nonlinear transient dynamic finite element simulations were performed using MSC.Dytran to aid in the design of an energy-absorbing impact sphere for a highly reliable, passive, Earth Entry Vehicle (EEV) that can survive a direct Earth impact without the aid of a

parachute. In addition, a methodology for modeling and simulating the highly complex materials used in the energy-absorbing impact sphere under impact conditions was presented.

In one possible architecture of the Mars Sample Return (MSR) mission, the collected samples contained within the EEV enter the Earth's biosphere and impact the Earth's surface, nominally in soft soil, at an estimated terminal velocity of 40 m/s. The EEV concept uses a hyperbolic entry capsule with an energy-absorbing impact sphere located inside the vehicle. The primary purpose of the impact sphere is to increase containment assurance and limit the acceleration of the collected samples housed within the orbiting sample (OS). The energy-absorbing impact sphere is a cellular structure composed of hybrid composite, graphite-epoxy/Kevlar cell walls filled with energy-absorbing carbon foam. The design of the cellular structure also includes a Kevlar outer shell and a graphite-Epoxy inner shell. Between the OS and cellular structure is the containment vessel (CV), which consists of woven Kevlar plies. The CV provides a second layer of containment and increases the impact resistance of the overall concept.

Impact tests of prototype cellular structures were performed for velocities of 30, 32, 35, and 40 m/s at the Impact Dynamics Research Facility (IDRF) at NASA Langley Research Center. For each impact test, a finite element model was created to simulate the event. Numerical data generated from impact simulations created using MSC.Dytran compared favorably with the impact test results for the four cellular structures. The finite element analyses predicted the shape, peak, and duration of the experimental acceleration; the rebound velocity; and the overall displacement and deformed shape of the cellular structure quite well.

The first impact simulation indicated that the cellular structure impact model had an excess of elastic energy, which produced a higher analytical rebound velocity than was

experimentally observed. With updates made to the second impact model, it was determined that the material model used to represent the foam cores was critical in predicting the impact loads on the OS and cellular structure. With the increased energy associated with the third impact model, proper yield and failure criteria for the cell walls was also determined to be critical in determining the accelerations observed in the OS and cellular structure. A FOAM1 material model for the foam cores and a 20% failure strain criterion for the cell walls gave an accurate prediction of the acceleration pulse, rebound velocity, and crush distance for the impact test specimen most representative of the planned flight vehicle velocity and mass.

When the cellular structure and OS were modeled as independent bodies, the acceleration of each component was complicated due to a two-body interaction. To evaluate the dynamic response of the cellular structure and make meaningful comparisons between analysis and test, a mass-weighted system acceleration of the cellular structure and OS was used. This method removed the interaction between the two bodies and provided the acceleration for the cellular structure at the center of mass. In addition, this comparison allowed the acceleration response of the impact test specimen to be determined for a "near perfect" coupling between the OS and cellular structure, expected for the flight vehicle where a spherical cellular structure and an optimized CV will be used.

Analytical models have proved useful as a tool for design and analysis of the cellular structure. In addition to modeling the impact tests performed at the IDRF, off-nominal impact studies were used to further the knowledge of the cellular structure concept. The off-nominal impact simulations consisted of various surfaces that the EEV, and possibly the cellular structure, could encounter upon impact with the Earth. These surfaces include the cellular structure impacting a flat surface with an angle of rotation, an angled surface representative of a

hill or large rock, and a corner of a step, representative of possible obstructions in the planned landing site. Results from these simulations indicate the need for further analysis to ensure that the dynamic loads transferred to the OS do not exceed the 3,500 g containment assurance limit. With the calibrated finite element model, additional off-nominal impact simulations can be performed that will provide guidance in the future design of the energy-absorbing impact sphere and the overall Earth Entry Vehicle.

13.0 Potential Research

The analysis of the cellular structure was performed to correlate the model with impact test data, to provide insight into the dynamic response of the cellular structure, and to perform off-nominal impact simulations. However, the finite element analysis was performed on the entire cellular structure and not on individual components. In particular, detailed analysis to determine the dynamic response of the bottom pentagonal cell under impact conditions would be beneficial. The foam and graphite-epoxy/Kevlar cell walls surrounding the bottom cell absorb a large amount of the energy stored in the cellular structure upon impact. Thus, fully understanding the energy absorption mechanisms in a single cell would allow for a better understanding of the entire cellular structure.

The energy absorbed by foam crushing inside a cell and deformation of the cell walls was addressed in the analytical models included for this research. Additional methods of energy dissipation not addressed by the current finite element model are the cell walls tearing from the outer Kevlar shell, the cell walls tearing apart at a corner, and the delamination of the composite cell walls. Breakable joints, constant force springs, and more accurate composite material models are all options that could be used to more accurately analyze a single cell, and thus the

cellular structure. However, for the analysis to be accurate, certain material properties need to be defined. The challenge is to devise testing methods to determine static and dynamic material properties needed for the impact simulation. A test program designed to meet the specific needs of the simulation would be required for meaningful analysis.

Additional component level analysis would be to determine the influence of the secondary containment vessel (CV) on the dynamic loads transferred to the OS. As observed in impact simulations #2 and #4, the soft, non-linear CV allowed relative motion between the OS and cellular structure that caused an amplification of the accelerations on the OS. The influence of CV on the cellular structure dynamic response needs additional study.

Other research areas related to this project would be to execute analyses of the cellular structure into the targeted impact area, the soft soil at UTTR. With a correlated cellular structure impact model and the soil finite element model described in reference [4], the two models could be merged to determine how the cellular structure dynamically responds in this type of impact simulation. The soft soil study [4] indicated that the ground would absorb a portion of the energy associated with the cellular structure impact and would most likely reduce the dynamic loads on the cellular structure.

Modeling and simulation of the entire Earth Entry Vehicle concept and determining how the entire system dynamically responds to a hard surface impact and/or a soft soil impact should be a subject of further analysis. This complete model would include a spherical cellular structure, an aeroshell, and the resulting support structure. At this time, there are multiple questions to be answered as to how these components will react to each other upon impact. A preliminary analysis would be beneficial to understanding the dynamics of the entire EEV structure.

14.0 References

1.) Mitcheltree, R. A., Kellas, S., Dorsey, P. N., Martin, C. J., "A Passive Earth-Entry Capsule for Mars Sample Return", AIAA 98-2851, 7th AIAA/ASME Joint Thermophysics and Heat Transfer Conference, Albuquerque, NM, June 1998

2.) Mitcheltree, R. A. and Kellas, S., "A Passive Earth-Entry Capsule for Mars Sample Return", Symposium on Atmospheric Reentry Systems, Arcachon France, March 1999.

3.) Mitcheltree, R., Braun, R., Hughes, S., Simonsen, L., "Earth Entry Vehicle for Mars Sample Return", IAF Paper 00-Q.3.04, Oct. 2000.

4.) Fasanella, E. L., Jones, Y. T., Knight, Jr., N. F., and Kellas, S., "Low Velocity Earth-Penetration Test and Analysis", AIAA 2001-1288, 42nd AIAA/ASME/ASCE/AHS/ASC Structures, Structural Dynamics, and Materials Conference and Exhibit, Seattle, WA, April 2001.

5.) Kellas, S., "Design Fabrication and Testing of a Crash Energy Absorber For a Passive Earth Entry Vehicle", EEV-2001-003, July 2001.

6.) MSC.Software Corporation, "MSC.Dytran Version 4.7 User's Manual", Volumes 1 and 2, Los Angeles, California, 1999.

7.) Vaughan, V. L. and Alfaro-Bou, E., "Impact Dynamics Research Facility for Full-Scale Aircraft Crash Testing", NASA TN D-8179, April 1976

8.) Desai, P. N., Mitcheltree, R. A., Cheatwood, F. M., "Sample Return Missions in the Coming Decade", IAF-00-Q.2.04, 51st International Astronautical Congress, Rio de Janeiro, Brazil, October 2000

9.) Hermann, R. J., and Lineberger, W. C., "Mars Sample Return: Issues and Recommendations", Task Group on Issues in Sample Return, Space Studies Board, National Research Council, ISBN 0-309-057337, National Academy of Sciences, 1997

10.) Carden, H. D., Kellas, S., "Composite Energy –Absorbing Structure for Aircraft Subfloors", Proceeding DOD/NASA/FAA Conference on Fibrous Composites in Structural Design, Volume II, South Carolina, November1993

11.) Kellas, S., "An Experimental Investigation into the Energy Absorption Performance of Composite Beam Webs for Aircraft Subfloor Applications", Proceeding of National Technical Specialists' Meeting on Rotorcraft Structures, "Design Challenges and Innovative Solutions", Sponsored by AHS, October 1995

12.) Kellas, S., Carden, H. D., "Crash-Energy Absorbing Composite Structure and Method of Fabrication", U.S. Patent # 5,746,537, May 5, 1998

13.) Kellas, S., Knight, N. F. Jr., "Design, Fabrication and Testing of Composite Energy-Absorbing Keel Beams for General Aviation Type Aircraft", AIAA 2001-1529, 42nd AIAA/ASME/ASCE/AHS/ASC Structures, Structural Dynamics, and Materials Conference and Exhibit, Seattle, WA, April 2001.

14.) Fasanella, E. L., Jackson, K. E., Kyle, K. H., "Crash Simulation of an Unmodified Lear Fan Fuselage Section Vertical Drop Test", Presented at the AHS 54th Annual Forum, Washington D.C., May 20-22, 1998.

15.) Jackson, K. E., Fasanella, E. L., "Crashworthy Evaluation of a 1/5-Scale Model Composite Fuselage Concept", Presented at the AHS 55th Annual Forum, Montreal, Canada, May 25-27, 1999.

16.) Fasanella, E. L., Jackson, K. E., Kyle, K. H., "Finite Element Simulation of a Full-Scale Crash Test of a Composite Helicopter", Presented at the AHS 56th Annual Forum, Virginia Beach, VA, May 2-4, 2000.

17.) Knight, N. F. Jr., Pinson, L. D., Kellas, S., "Composite Subfloor Beam Simulations Using MSC/Dytran", NASA Final Report for Task 1408, Subtask 1, September 1999

18.) Knight, N. F. Jr., Kellas, S., Pinson, L. D., "Predicting the Impact Response of an Energy-Absorbing Composite Subfloor Beam", AIAA 2000-1472, 41st AIAA/ASME/ASCE/AHS/ASC Structures, Structural Dynamics, and Materials Conference and Exhibit, Seattle, WA, April 2000.

19.) MSC.Software Corporation, "Introduction to MSC.Dytran Seminar Notes", MSC.Dytran Course – DYT101, Los Angeles, California, 1999.

20.) Fasanella, E. L., Billings, M. D., "Dynamic Finite Element Predictions for Mars Sample Return Cellular Impact Test #4", NASA/TIM-2001-211023, ARL-TR-2539, March 2001

21.) Billings, M. D., Fasanella, E. L., Kellas, S., "Impact Test and Simulation of Energy Absorbing Concepts for Earth Entry Vehicles", AIAA 2001-1602, 42nd AIAA/ASME/ASCE/AHS/ASC Structures, Structural Dynamics, and Materials Conference and Exhibit, Seattle, WA, April 2001.

REPORT DOCUMENTATION PAGE

Form Approved
OMB No. 0704-0188

1. AGENCY USE ONLY (*Leave blank*)	2. REPORT DATE	3. REPORT TYPE AND DATES COVERED
	May 2002	Contractor Report

4. TITLE AND SUBTITLE
Analytical Simulations of Energy-Absorbing Impact Spheres for a Mars Sample Return Earth Entry Vehicle

5. FUNDING NUMBERS
C NCC1-01017
WU 728-50-10-01

6. AUTHOR(S)
Marcus Dwight Billings

7. PERFORMING ORGANIZATION NAME(S) AND ADDRESS(ES)
The George Washington University
Joint Institute for Advancement of Flight Sciences
NASA Langley Research Center
Hampton, VA 23681-2199

8. PERFORMING ORGANIZATION REPORT NUMBER

9. SPONSORING/MONITORING AGENCY NAME(S) AND ADDRESS(ES)
National Aeronautics and Space Administration
Langley Research Center
Hampton, VA 23681-2199

10. SPONSORING/MONITORING AGENCY REPORT NUMBER
NASA/CR-2002-211671

11. SUPPLEMENTARY NOTES
The information presented in this report was submitted to the School of Engineering and Applied Science of The George Washington University in partial fulfillment of the requirements for the Degree of Master Science, April 2002. Langley Technical Monitor: Edwin L. Fasanella

12a. DISTRIBUTION/AVAILABILITY STATEMENT
Unclassified-Unlimited
Subject Category 05 Distribution: Standard
Availability: NASA CASI (301) 621-0390

12b. DISTRIBUTION CODE

13. ABSTRACT *(Maximum 200 words)*
Nonlinear dynamic finite element simulations were performed to aid in the design of an energy-absorbing impact sphere for a passive Earth Entry Vehicle (EEV) that is a possible architecture for the Mars Sample Return (MSR) mission. The MSR EEV concept uses an entry capsule and energy-absorbing impact sphere designed to contain and limit the acceleration of collected samples during Earth impact without a parachute. The spherical shaped impact sphere is composed of solid hexagonal and pentagonal foam-filled cells with hybrid composite, graphite-epoxy/Kevlar cell walls. Collected Martian samples will fit inside a smaller spherical sample container at the center of the EEV's cellular structure. Comparisons were made of analytical results obtained using MSC.Dytran with test results obtained from impact tests performed at NASA Langley Research Center for impact velocities from 30 to 40 m/s. Acceleration, velocity, and deformation results compared well with the test results. The correlated finite element model was then used for simulations of various off-nominal impact scenarios. Off-nominal simulations at an impact velocity of 40 m/s included a rotated cellular structure impact onto a flat surface, a cellular structure impact onto an angled surface, and a cellular structure impact onto the corner of a step.

14. SUBJECT TERMS
Mars Sample Return Program, Earth Entry Vehicle, dynamic finite element analysis, composite structural impact, MSC.Dytran, dynamic structural analysis

15. NUMBER OF PAGES
86

16. PRICE CODE

17. SECURITY CLASSIFICATION OF REPORT	18. SECURITY CLASSIFICATION OF THIS PAGE	19. SECURITY CLASSIFICATION OF ABSTRACT	20. LIMITATION OF ABSTRACT
Unclassified	Unclassified	Unclassified	UL